CLPP-Null Eukaryotes with Excess Heme Biosynthesis Show L-arginine Reduction, Probably via CLPX-Mediated OAT Activation

Jana Key , Suzana Gispert , Daniela Heinz , Andrea Hamann , Heinz D. Osiewacz , David Meierhofer , Georg Auburger *

Posted Date: 19 January 2024

doi: 10.20944/preprints202401.1423.v1

Keywords: Perrault Syndrome; PLP; metal homeostasis; delta amino acids

Article

CLPP-Null Eukaryotes with Excess Heme Biosynthesis Show L-Arginine Reduction, Probably via CLPX-Mediated OAT Activation

Jana Key [1], Suzana Gispert [1], Daniela Heinz [2], Andrea Hamann [2], Heinz D. Osiewacz [2], David Meierhofer [3] and Georg Auburger [1]

[1] Goethe University Frankfurt, University Hospital, Clinic of Neurology, Exp. Neurology, Heinrich Hoffmann Str. 7, 60590 Frankfurt am Main, Germany; Jana.Key@kgu.de; Gispert-Sanchez@em.uni-frankfurt.de; Auburger@em.uni-frankfurt.de

[2] Institute of Molecular Biosciences, Faculty of Biosciences, Goethe-University, Frankfurt, Germany; osiewacz@bio.uni-frankfurt.de; a.hamann@bio.uni-frankfurt.de; dheinz089@gmail.com

[3] Max Planck Institute for Molecular Genetics, Ihnestraße 63-73, 14195 Berlin, Germany; meierhof@molgen.mpg.de

* Correspondence: auburger@em.uni-frankfurt.de

Abstract: Serine peptidase CLPP is conserved among bacteria, chloroplasts, and mitochondria. In humans and mice, its loss causes Perrault syndrome with growth deficit, infertility, deafness, and ataxia. In the filamentous fungus *Podospora anserina*, CLPP-loss leads to longevity. CLPP substrates are selected by CLPX, an AAA+ unfoldase. CLPX is known to target delta-amino-levulinic-acid synthase (ALAS) to promote pyridoxal-phosphate (PLP) binding. CLPX may influence cofactor association with other enzymes. Here, the evaluation of *P. anserina* metabolomics highlighted arginine/histidine reduction. In *Mus musculus* cerebellum, reductions of Arginine/Histidine and Citrulline occurred with concomitant accumulation of heme-precursor protoporphyrin-IX. This suggests that increased biosynthesis of 5-carbon (C5) chain deltaALA consumes not only C4 succinyl-CoA with C1 glycine but also specific C5 delta amino-acids. As responsible enzymes for these converse effects, elevated abundance of CLPX and ALAS is paralleled by elevation of OAT (PLP-dependent, ornithine-delta-aminotransferase). Possibly as consequence of altered C1 metabolism, CLPP-null cells in *P. anserina* proteome profiles showed strong accumulation of a methyltransferase and two mitoribosomal large subunit factors. Reduced Histidine levels may explain previously observed metal interaction problems. As main nitrogen-storing metabolite, deficient Arginine would affect the urea cycle and polyamine synthesis. Supplementation of Arginine and Histidine might rescue growth deficits of CLPP-mutant patients.

Keywords: Perrault Syndrome; PLP; metal homeostasis; delta amino acids

1. Introduction

Bacterial ClpP (ATP-dependent caseinolytic serine peptidase, proteolytic subunit, also named "endopeptidase Ti" in *Escherichia coli* bacteria) cleaves peptide bonds between carboxy groups and amino groups. In the presence of ATP and magnesium, it can degrade proteins such as casein [1]. The strong conservation of ClpP (around 50% amino acid identity [2]) from bacteria to chloroplasts and mitochondria has enabled the unequivocal demonstration of its crucial role in cell stress responses [3,4]. However, its degradation targets are still under debate given that bulk protein breakdown in mitochondria depends more on LonP than ClpP orthologs across evolution [5,6]. Further insights into the role of ClpP may be derived from the fact that it depends on an AAA+ disaggregase for substrate selection and ATP hydrolysis. This unfolding and chaperone function is usually performed by ClpX, but in some bacterial strains by ClpA-E. The abundance of this AAA+ disaggregase correlates inversely with ClpP protein levels [3,7,8], so absent ClpP functions might be compensated by high ClpX activity.

In *Saccharomyces cerevisiae* yeast, a CLPP ortholog has not been identified, while the ClpX orthologous protein MCX1 is abundant. MCX1 does not contain the conserved IGF domain for CLPP

 doi:10.20944/preprints202401.1423.v1

interaction, so yeast CLPX is thought to act as pure unfoldase/chaperone without associated substrate cleavage. Its function was found to be crucial, mediating activation of the initial step in heme biosynthesis: MCX1 unfolds delta-amino-levulinic-acid (δALA, deltaALA, or simply ALA) synthase enzyme (ALAS) and catalyzes the incorporation of its cofactor, pyridoxal-5'-phosphate (PLP or P5P, the active form of vitamin B6), which is needed for efficient transamination. δALA constitutes the building block for tetrapyrrol rings with downstream porphyrins, which can chelate Fe^{2+} or Mg^{2+} to yield heme or chlorophyll, respectively (Figure 1). In archaea/bacteria, δALA is also the building block for the biosynthesis of corrin rings from porphobilinogen, which can chelate Co^{2+} to yield cobalamin (vitamin B12) as a crucial cofactor of enzymes. In mammals, two enzymes require cobalamin-binding (methionine synthase and methylmalonyl-CoA mutase). They control mitochondrial C1 metabolism, S-adenosyl-methionine (SAM)-dependent methylations, and epigenetics [9].

The role of CLPX for ALAS activation via PLP association is highly conserved from yeast to humans. The deletion of yeast CLPX leads to a 5-fold reduction of δALA and to a reduction of heme by half [10]. In the zebrafish *Danio rerio*, phenotypes due to the depletion of CLPX can be compensated by the administration of δALA [11]. In *Homo sapiens*, mutations in CLPX trigger hematological disorders due to errors in heme biosynthesis [12,13]. ALAS synthesizes the non-proteinogenic δALA from succinyl-coenzyme-A (succinyl-CoA) and the proteinogenic amino acid glycine (see Figure 1). This biosynthesis pathway of the five-carbon (C5) compound δALA from the four-carbon (C4) source succinyl-CoA and adding glycine (as described by Shemin and coworkers [14]) is predominant in animals, fungi, protozoa, and alphaproteobacteria as ancestors of mitochondria.

A more ancient mechanism for δALA biosynthesis (defined by Beale and coworkers [15], see Figure 1) uses C5 acids (alpha-ketoglutarate or rather its transaminated form, glutamate). This pathway is prominent in archaea, most bacteria, algae, and plants. Several microorganisms use both C4 and C5 substrates [16,17]. In this C5 pathway, δALA is produced by a chain of 3 enzymes (GltX, HemA, HemL), with the final step from glutamate-1-semi-aldehyde (GSA, or better G1SA) done by the PLP-activated enzyme HemL (also known as GSA 2,1-aminomutase, or GSA aminotransferase). For HemA, there is no ortholog in animals, so δALA production from glutamyl-tRNA cannot occur, and therefore it has been argued that the C5 / Beale pathway cannot be used in eukaryotes. Indeed, the nitrogen from glycine is used for heme biosynthesis in mammals under normal conditions rather than glutamate/GSA, according to isotope-labelled metabolism studies [14], but this does not exclude that a pathological overactivation of δALA production due to CLPX excess might recruit additional nitrogen sources such as GSA. It is conceivable that HemA became unnecessary in eukaryotes because GSA can be produced from other sources and might be converted to δALA by a homolog of HemL. Bacterial HemL has significant sequence-homology in *P. anserina* (PODANS) with PODANS_5_6860 (GSA 2,1-aminomutase), but also with PODANS_7_10880 (ornithine-delta-aminotransferase, or OAT), and with the aminotransferases PODANS_6_1290, PODANS_7_5560, PODANS_3_9430, according to the STRING Heidelberg webserver. In mice, HemL homology is significant principally for OAT, but also for PHYKPL (5-phosphohydroxy-L-lysine phospho-lyase), ETNPPL (ethanolamine-phosphate phospho-lyase), AGXT2 (alanine-glyoxylate aminotransferase 2) and ABAT (4-aminobutyrate aminotransferase), all of which require PLP as cofactor. We might therefore hypothesize that in mammals, OAT-PLP facilitate the production of δALA via GSA that is derived directly from ornithine / arginine rather than more indirectly from glutamate / alpha-ketoglutarate (see Figure 1). Recently, members of our Frankfurt team reported endogenous levels of OAT and CLPX to interact in coimmunoprecipitation analyses of CLPP-mutant cells and observed pathological accumulation of iron and cobalt in these cells [18]. Therefore, OAT might be unfolded by CLPX to use PLP in an analogous manner as ALAS, contributing to excessive production of heme (in eukaryotes) and cobalamin (in archaea/bacteria).

Preprints (www.preprints.org) | NOT PEER-REVIEWED | Posted: 19 January 2024 doi:10.20944/preprints202401.1423.v1

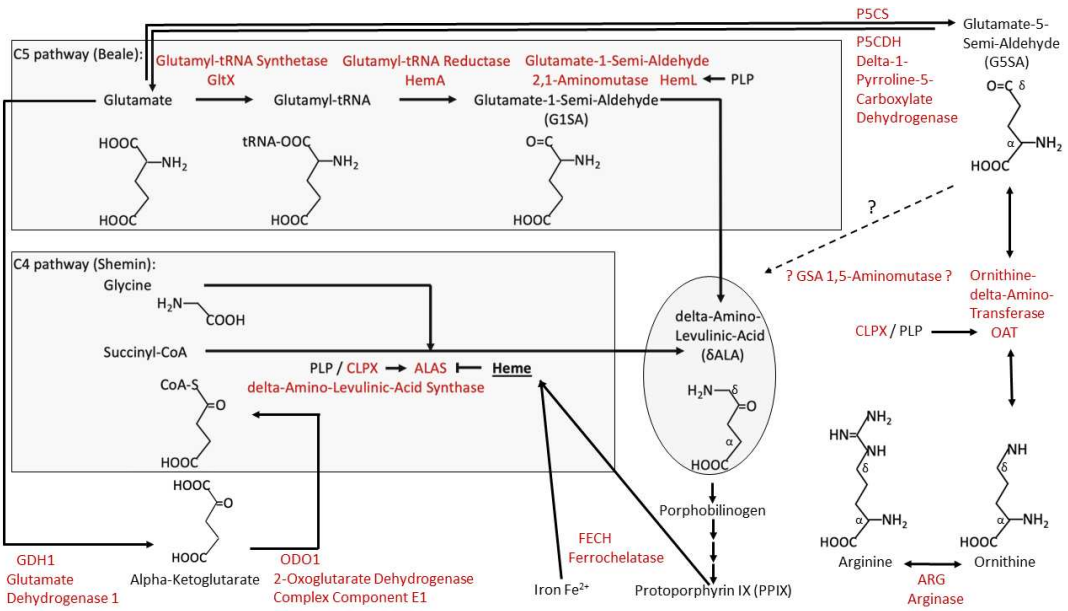

Figure 1. For the mitochondrial biosynthesis of heme from protoporphyrin-IX and iron, a symmetric tetrapyrrole ring system has to be generated, from the building block delta-amino-levulinic-acid (δALA, or simply ALA). The production of this non-cognate amino acid occurs predominantly via the C5 pathway in archaea / plants, versus the C4 pathway in fungi / animals. According to the present study, overactivity of CLPX/ALAS and CLPX/OAT in two models of PRLTS3 pathogenesis reduces arginine like glycine in CLPP-null *P. anserina*, and arginine stronger than serine in CLPP-null mouse cerebellum, presumably via G5SA consumption. Whether the sequence homology and structural similarity between OAT and GSA-Aminomutase reflects an ancient processing of ornithine as C5-substrate into δALA-biosynthesis, remains to be tested further and is highlighted by question marks. Arrows reflect metabolic flux, and CLPX/PLP-activation of ALAS/OAT, versus ALAS repression by end-product heme. Enzymes and their protein symbols are shown in red letters. P5CS represents delta-1-pyrroline-5-carboxylate-synthase, synonymously known as ALDH18A1 (aldehyde dehydrogenase 18 family member A1).

What is PLP needed for? Coexisting with RNA since the prebiotic world [19], PLP became useful in the optimized biosynthesis and degradation of amino acids, via its protein association first as a chaperone [20] and then as a cofactor of enzymes. It is required for all transaminations, some decarboxylations, dehydrations, and racemizations, but can also modulate desulfurizations [21]. The main role of PLP in the metabolism of cognate proteinogenic amino acids with their amino group at the alpha-carbon position does not appear to depend on CLPX unfolding functions. However, PLP also acts as a key cofactor in the metabolism of non-cognate amino acids that are derived from arginine, e.g. its blood pressure signaling derivatives like alpha-keto-delta-(N,N-dimethylguanidino)-valeric-acid, and its non-proteinogenic precursors citrulline / ornithine and its non-proteinogenic analogue homoarginine. Furthermore, PLP is a cofactor in the generation of non-canonical amino acids that act as (i) detoxifiers (like cystathionine, glutathione and the polyamines putrescine-spermidine-spermine, with their derivative hypusine that is required for ribosomal fidelity during translation elongation across poly-proline sequences [22,23]), (ii) messengers (like gamma-amino-butyric-acid or GABA), and (iii) toxins (like ibotenic acid) [24,25]. All such metabolites are derived from classical amino acids but have an amino group away from the carboxylic-acid group at delta- or gamma-position. Therefore, the aminotransferase domain with bound PLP would need to act at a δ- or γ-carbon (see Figure 1 for Arg, Orn amino groups, and for the change of the amino group from the α-carbon in G1SA to the δ-carbon in δALA which would require an aminomutase function). Any enzyme that acts as transaminase or aminomutase at δ-carbons might need CLPX-mediated unfolding, if it is docked at the carboxy group to reach across this distance [26].

In *Caenorhabditis elegans* nematode worms, CLPP depletion was observed to have a prominent impact on the cellular response to unfolded protein stress within mitochondria (UPR^{mt}) [27], a

 doi:10.20944/preprints202401.1423.v1

retrograde signaling pathway from mitochondria to the nucleus that regulates transcription factors like ATF4 [28]. Similarly, the overexpression of CLPX in mammalian cells was also reported to activate the UPR^{mt} pathway [29]. As an underlying mechanism in bacteria and mammalian cells, it was shown that the stalling of ribosomal translation triggers a polypeptide chain elongation with an alanine-threonine-rich tail, which is recognized by CLPX and results in the elimination of this misfolded protein fragment by CLPP [30–32]. Ribosomal stalling and nascent peptide misfolding are frequent events during protein synthesis, usually due to the presence of poly-proline motifs [33] or other ribosomal translation fidelity problems [34,35]. Thus, the CLPXP pathway has a quality surveillance function for mitochondrial polypeptide chains.

Human data showed the loss-of-function of CLPP to cause phenotypes classified as Perrault syndrome type 3 (PRLTS3) [36]. The original definition of Perrault syndrome was based on its autosomal recessive inheritance, and on the co-occurrence of primary ovarian insufficiency with subsequent deafness [37]. PRLTS3 patients in addition show strong body height reduction [36] and weight deficits, as well as an age-associated widespread nervous system atrophy that includes ataxia, neuropathy, and leukodystrophy [38]. The proteome profiling of PRLTS3 patient fibroblasts confirmed several-fold CLPX accumulation as the most consistent consequence of CLPP loss-of-function [39]. Most other causes of Perrault syndrome are due to mutant genes that encode components of the mitochondrial RNA processing or translation pathway, such as the nucleoid replication/repair factor TWNK, the RNA degradation factor PRORP, the tRNA-amino-acid-synthases HARS2 and LARS2, and the mitoribosomal factor RMND1 [40,41]. How these phenotypes and a mitoribosomal pathology can be mechanistically explained given specific heme production problems and possibly multiple other CLPX-PLP-associated enzyme alterations, remains enigmatic.

Small drugs that are in clinical use to counteract bacterial infections were found to inhibit or activate CLPP and later reported to also affect the viability and proliferative activity of carcinomas [42]. Several CLPP agonists (ONC201 as well as other imipridones) were demonstrated to be quite efficient not only against bulk tumor cells, but also cancer stem cells, cancer-associated fibroblasts, and immune cells within the tumor microenvironment. ONC201 as a single agent is useful for subtypes of high-grade glioma, endometrial cancer, prostate cancer, mantle cell lymphoma, and adrenal tumors [43]. Other CLPP agonists are being evaluated for leukemia treatment [44]. Even more, a detailed understanding of the impact of CLPP on mitochondrial metabolism is urgently needed.

In CLPP-null mice as PRLTS3 model, both females and males are completely infertile [45], a growth deficit despite increased food consumption decreases body length by 10% and weight by 30%, with 64% reduction in fat mass versus 24% reduction in lean mass [46,47], and deafness occurs by the age of 1 year [8]. Similar to bacteria and human cells, in mouse tissues the primary consequence of CLPP absence is the >3-fold accumulation of CLPX [8]. The abundance of CLPX increases together with its interacting mitochondrial nucleoid proteins and mtDNA [39], and with ribonucleoproteins, particularly from the mitoribosomal large and small subunit (LSU, SSU) or translation elongation machinery [48]. The consequent mitochondrial dysfunction activates the innate immune defenses and leads to protection from bacterial infections, such as *dermatitis ulcerosa* [8,49–51]. Given that the CLPP-null mouse mutant is an authentic model of PRLTS3 patient phenotypes, we now used its brain tissue for in-depth studies of the mitochondrial amino-acid metabolism, taking advantage of the fact that the blood-brain barrier shelters the nervous system from the feeding-related fluctuations in nutrient availability. Adult cerebellar tissue was chosen as the area where ataxia phenotypes are usually triggered, and because of its uniform structure. To elucidate the consistency of CLPP effects across evolution, this approach was complemented by the analysis of a fungal eukaryote during an early stage (at day 8) of its life cycle.

The filamentous fungus *Podospora anserina* is characterized in much detail as a model organism for aging research. Its usefulness is due to its short lifespan (normally around 3-5 weeks), a phenotypically obvious senescence stage, and several isolates with altered survival due to mutations, which can be easily generated by molecular genetics in this organism [52,53]. In contrast to humans, which are diplonts with two homologous chromosomes and thus two alleles for every gene, *P.*

 doi:10.20944/preprints202401.1423.v1

anserina is a haplont with a single chromosome set, possibly explaining different phenotypes caused by identical mutations in these two organisms.

The genetic deletion of CLPP was shown to prolong *P. anserina* (*Pa*) healthy lifespan 2-3-fold, and this effect could be extended much by additional deletion of the i-AAA mitochondrial inner membrane protease (*ΔPaIap*). Human CLPP was able to substitute for PaCLPP and revert the phenotype [54]. The combined deletion of CLPP and AMP kinase (*ΔPaClpP/ΔPaSnf1*) extends a healthy lifespan by more than 500% at 27 °C under constant light for a specific mating type, an effect that was lost upon high-temperature stress [55].

Two published reports on *P. anserina* CLPP-null strains underlie the present project. Regarding the metabolomics profile of the *ΔPaClpP* strain at 5 and 20 days of growth, low levels were reported for most amino acids, phosphoenolpyruvate, and ATP/GTP/CTP/UTP at a young age, followed by unexpectedly high levels of these metabolites in later life [55]. In a further study to identify CLPP cleavage substrates, catalytically inactive HsCLPP-S153A was introduced in the *ΔPaClpP* strain, a failure of phenotype reversion was demonstrated, and 47 mitochondrial proteins co-purified with wildtype and mutant CLPP as potential interactors, while 19 mitochondrial proteins co-purified selectively with mutant CLPP as putative degradation targets [56]. A bioinformatic gene ontology term analysis (GO-term analysis) assigned these potential CLPP interaction partners and substrates to different mitochondrial processes and pathways such as the respiratory chain, the TCA cycle, members of the chaperone system, or amino-acid metabolism. Strikingly, components of the N-module of respiratory chain complex I appear to be conserved CLPP substrates among species such as *P. anserina*, *Arabidopsis thaliana,* and mice [2,56–58].

To elucidate the impact of these findings in more detail and to identify evolutionarily conserved molecular pathways controlled by CLPP, we re-analyzed the *P. anserina* metabolome and protein-interaction data, complemented them with global proteome profile data of an 8 days-old CLPP-null *P. anserina* mutant, and with data from adult mouse cerebellum. Finally, we asked the question if CLPP absence via excess CLPX might modulate the PLP-binding of additional mitochondrial enzymes beyond ALAS, thus modulating the levels of cognate and non-cognate amino acids, and in parallel also TCA cycle intermediate metabolites.

2. Materials and Methods

2.1. Culture conditions of P. anserina:

The media used in this study can be found in [55].

2.2. Metabolic Profiling of P. anserina:

The metabolic profiling has been described in [55]. In short, four biological replicates of 5- and 20-day-old wildtype and CLPP-null strains were used for metabolic profiling by Metabolomic Discoveries (Metabolomic Discoveries GmbH, Potsdam, Germany).

2.3. Global proteome profile of P. anserina:

Wildtype and CLPP-null strains were germinated for two days, grown on M2 medium (three days), and inoculated in CM liquid medium (0.1% KH_2PO_4, 0.05% KCl, 0.05% $MgSO_4$, 1% glucose, 0.37% NH_4Cl, 0.2% tryptone, 0.2% yeast extract, 0.1% stock solution A) for additional three days with shaking in constant light. This stock solution A consists of 0.1% $ZnSO_4$, 0.1% $FeCl_2$, 0.1% $MnCl_2$, pH 6.5 (KOH). After total protein extraction [55], 20 µg protein (in 16.5 µl) was mixed with 3.5 µl SDS-loading buffer (6% Tris/HCl pH 6.8, 48% glycerol, 9% ß-mercapto-ethanol, 0.03% bromophenol blue, 6% SDS). After boiling (10 min, 95 °C) and cooling on ice, samples were stored at –20 °C. Later, 20 µg of protein were separated in 4-12% gradient Novex Bis-Tris gels (LifeTechnologies, Carlsbad, CA, USA). SDS-PAGE was stopped after proteins entered the first 0.5 cm of the separating gel. Gels were fixed in 50% (v/v) methanol, 10% (v/v) acetic acid, 10 mM ammonium acetate for 30 min and stained with Coomassie (0.025% Serva Blue G, 10% (v/v) acetic acid). Gel was cut into 4 fractions and collected in 96 filter well plates (30-40 µm PP/PE, Pall Corporation, Port Washington, NY, USA). The gel pieces

 doi:10.20944/preprints202401.1423.v1

were destained in 60% methanol, 50 mM ammonium bicarbonate (ABC). Solutions were removed by centrifugation for 2 min at 600 g. Proteins were reduced in 10 mM DTT, 50 mM ABC for one hour at 56 °C, and alkylated for 45 min in 30 mM iodoacetamide. Samples were digested for 16 h with trypsin (sequencing grade, Promega, Madison, WIS, USA) at 37 °C in 50 mM ABC, 0.01% Protease Max (Promega) and 1 mM $CaCl_2$. Peptides were eluted in 30% acetonitrile and 3% formic acid, centrifuged into a fresh 96 well plate, dried in speed vac, and resolved in 1% acetonitrile and 0.5% formic acid.

Liquid chromatography / mass spectrometry (LC/MS) was performed on Thermo Scientific™ Q Exactive Plus equipped with an ultra-high performance liquid chromatography unit (Thermo Scientific Dionex Ultimate 3000) and a Nanospray Flex Ion-Source (Thermo Scientific, Waltham, MA, USA). Peptides were loaded on a C18 reversed-phase precolumn (Thermo Scientific) followed by separation on a with 2.4 µm Reprosil C18 resin (Dr. Maisch GmbH, Ammerbuch, Germany) in-house packed picotip emitter tip (diameter 100 µm, 15 cm from New Objectives, Littleton, MA, USA) using a gradient from mobile phase A (4% acetonitrile, 0.1% formic acid) to 50 % mobile phase B (99% acetonitrile, 0.1% formic acid) for 30 min with a flow rate 400 nl/min and washout with 99% B for 5 min.

MS data were recorded by data-dependent acquisition. The full MS scan range was 300 to 2000 m/z with a resolution of 70,000, and an automatic gain control (AGC) value of 3×10^6 total ion counts with a maximal ion injection time of 160 ms. Only higher charged ions (2+) were selected for MS/MS scans with a resolution of 17,500, an isolation window of 2 m/z and an automatic gain control value set to 10^5 ions with a maximal ion injection time of 150 ms. MS1 data were acquired in profile mode.

MS data were analyzed by MaxQuant (v1.6.1.0) using default settings. Proteins were identified using proteome database UniProtKB with 10,657 entries, released in 8/2018. The enzyme specificity was set to Trypsin. Acetylation (+42.01) at N-terminus and oxidation of methionine (+15.99) were selected as variable modifications and carbamidomethylation (+57.02) as fixed modification on cysteines. False discovery rate (FDR) for the identification protein and peptides was 1%.

Label-free quantification values were obtained from at least one identified peptide. Identifications from reverse decoy database, by site and known contaminants were excluded. Data were further bioinformatically analysed by Perseus 1.6.1.3. and Microsoft Excel. For quantification proteins were quality filtered according to a minimum of 3 valid values in one group (n=3). All missing values from this reduced matrix were replaced by the background value representing half of the lowest value in the dataset. For statistical comparison, Student's t-tests and permutation-based FDR were used. The mass spectrometry proteomics data have been deposited to the ProteomeXchange Consortium via the PRIDE partner repository with the dataset identifier PXD048640.

2.4. Mouse cerebellar metabolome:

For the quantification of metabolic compounds in 12-month-old mouse cerebellum, 8 WT versus 8 CLPP-null sex-matched tissues were snap frozen in liquid nitrogen, stored at −80 °C, and shipped on dry ice to the company Metabolomic Discoveries (Potsdam, Germany). Targeted profiling with unambiguous characterization and relative quantification by LC-tandem mass spectrometry was performed on a Shimadzu (Kyoto, Japan) triple quadrupole LCMS-8050 equipped with an electrospray ionization (ESI) source and operated in multiple reaction mode (MRM). For statistical evaluation, raw data as peak abundances normalized to internal standards and, if necessary, protein content were detailed, complemented by means and standard deviation values, as well as a differential analysis sheet with ANOVA across all groups as a global p-value, and an adjusted global p-value, followed by a local p-value from pairwise t-tests and ratios of the group means as a $\log_2$ value, as well as absolute fold changes.

 doi:10.20944/preprints202401.1423.v1

2.5. Mouse metabolic validation study:

The whole cerebella from 10 WT versus 10 CLPP-null 12-month-old sex-matched mice were snap-frozen in liquid nitrogen and stored at −80 °C until further processing. Metabolite extraction and tandem LC-MS/MS measurements were done as previously reported by us [59]. In brief, methyl-tert-butyl ester (MTBE, Sigma-Aldrich, St. Louis, MO, USA), methanol, ammonium acetate, and water were used for metabolite extraction. Subsequent separation was performed on an LC instrument (1290 series UHPLC; Agilent, Santa Clara, CA, USA), online coupled to a triple quadrupole hybrid ion trap mass spectrometer QTrap 6500 (Sciex, Foster City, CA, USA), as reported previously [60]. Metabolomics data have been deposited in the publicly available repository PeptideAtlas with the identifier PASS05856 and can be downloaded via http://www.peptideatlas.org/PASS/PASS05856.

The metabolite identification was based on three levels: (i) the correct retention time, (ii) up to three MRMs (iii) and a matching MRM ion ratio of tuned pure metabolites as a reference. Relative quantification was performed using MultiQuantTM software v.2.1.1 (Sciex, Foster City, CA), and all peaks were reviewed manually. Only the average peak area of the first transition was used for calculations. Normalization was based on the protein concentration of the samples and subsequently by internal standards.

2.6. Statistical analyses

For statistical analyses, Microsoft Excel was used. Volcano plots were generated with Graphpad Prism, Version 10.

3. Results

3.1. Re-analysis of CLPP-mutation effects in P. anserina:

For the purpose of the present study into the PLP-dependent metabolism of amino acids, it is first important to reconsider the previous trap-assay study in *P. anserina* [56].

(i) Among the 47 putative CLPP interacting proteins identified [56], there are six that are known for their association with PLP, namely the ornithine delta-aminotransferase OAT, the aspartate aminotransferase GOT2, the branched-chain amino-acid aminotransferase BCAT2, the glycine decarboxylase GLDC, the serine hydroxymethyltransferase SHMT2, and the cysteine desulfurase NFS1.

(ii) Among the 19 potential CLPP degradation substrates identified in this study [56], only CLPX associates with PLP, while most other candidate CLPP cleavage targets have cofactors like lipoate, FeS clusters, thiamine diphosphate, or FAD. Therefore, excess CLPX in CLPP-mutant organisms might modulate also other PLP-associated enzymes beyond ALAS, and the binding of other cofactors might be relevant for CLPP cleavage.

Next, it is important to reflect on the metabolic profile of CLPP-null *P. anserina* during aging. In contrast to the progressive accumulations of phosphoenolpyruvate and most amino acids from day 5 to 20 in the lifespan, pyruvate stood out with low levels that increased over time, and ornithine appeared prominent with low levels that decreased more over time [55]. The metabolite ornithine is in flux equilibrium (i) via the mitochondrial matrix enzyme OAT with glutamate-5′-semialdehyde (GSA or better G5SA) and Δ-1-pyrroline-5-carboxylate (P5C) as precursors of glutamate or proline, respectively (see Figure 2), (ii) via the mitochondrial matrix enzyme ornithine transcarbamylase (OTC) with citrulline as precursor of arginine, and (iii) via the cytosolic enzyme ornithine decarboxylase (ODC or ODC1) with the polyamine putrescine as precursor of spermidine / hypusine or spermine (see Figure 2). It was previously shown in plants that OAT is crucial for ornithine generated by arginine breakdown in the urea cycle, but it is not necessary for proline biosynthesis [61], so its primary role is the generation of G5SA.

Preprints (www.preprints.org) | NOT PEER-REVIEWED | Posted: 19 January 2024 doi:10.20944/preprints202401.1423.v1

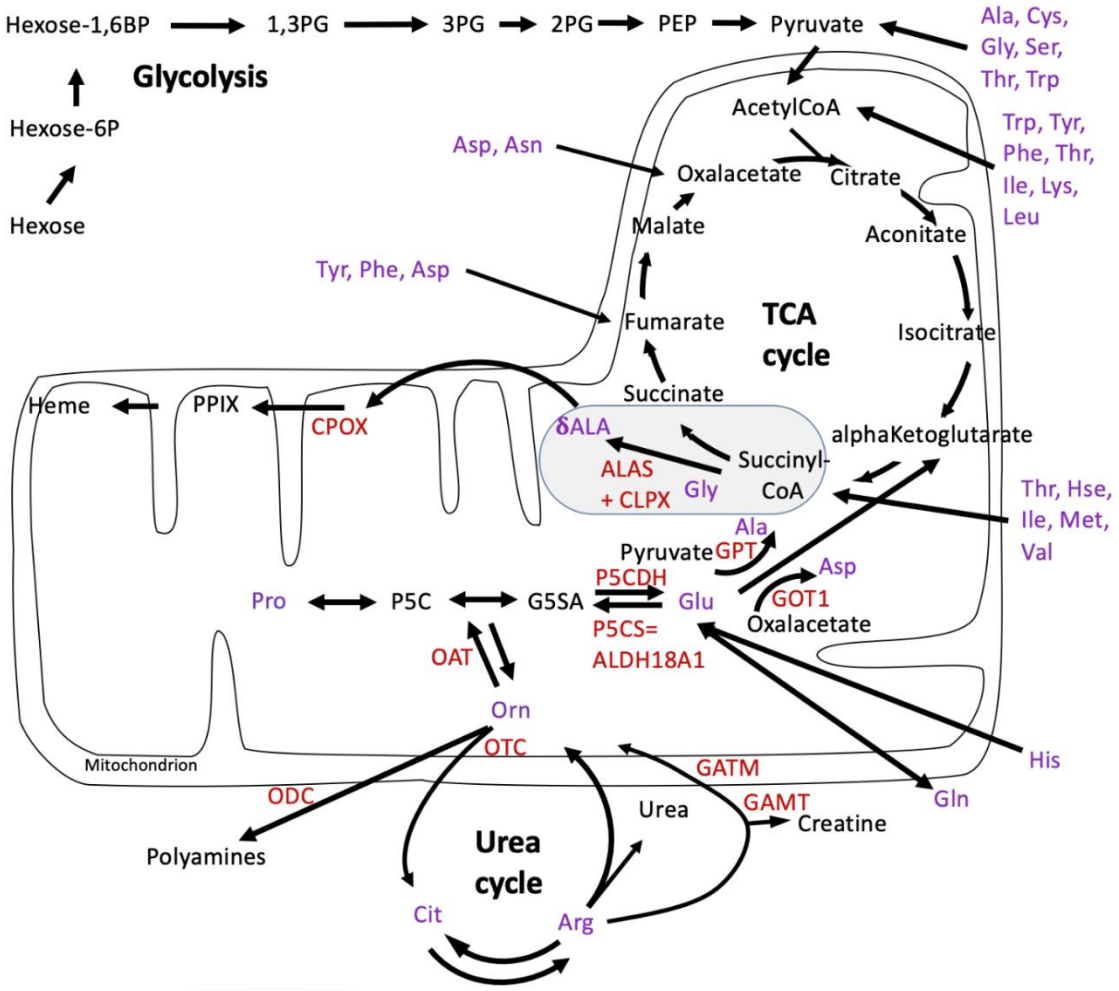

Figure 2. Breakdown of amino acids for consumption in the mitochondrial TCA cycle, and extra-mitochondrial metabolite flux from urea cycle and glycolysis towards heme biosynthesis in wildtype cells. The scheme was modified from the biochemistry textbook Stryer and from [62]. The well-established Shemin pathway of heme biosynthesis is highlighted in an ellipse with a gray background. Enzymes are shown in auburn (red-brown) letters: ALAS = delta-amino-levulinic-acid synthase; CLPX = caseinolytic mitochondrial matrix peptidase chaperone subunit X; CPOX = coproporphyrinogen oxidase; GAMT = guanidinoacetate N-methyltransferase; GATM = glycine amidinotransferase; GOT1 = glutamic-oxaloacetic transaminase 1; GPT = glutamic-pyruvic transaminase; OAT = ornithine delta-aminotransferase; ODC = ornithine decarboxylase; OTC = ornithine transcarbamylase; P5CDH = pyrroline-5-carboxylate dehydrogenase; P5CS = pyrroline-5-carboxylate synthetase = ALDH18A1 = aldehyde dehydrogenase 18 family member A1. Amino acids are shown in purple letters: Ala = alanine; δALA = delta-amino levulinic acid; Arg = arginine; Asn = asparagine; Asp = aspartate; Cit = citrulline; Cys = cysteine; Gln = glutamine; Glu = glutamine; Gly = glycine; His = histidine; Hse = homoserine; Ile = isoleucine; Leu = leucine; Lys = lysine; Met = methionine; Orn = ornithine; Phe = phenylalanine; Pro = proline; Ser = serine; Thr = threonine; Trp = tryptophan; Tyr = tyrosine; Val = valine. Other metabolites are shown in black letters: CoA = coenzyme A; Hexose-6P = hexose-6-phosphate; Hexose-1,6BP = hexose-1,6-bisphosphate; 1,3PG = 1,3-bisphospho-glycerate; 2PG = 2-phosphoglycerate; 3PG = 3-phosphoglycerate; PEP = phosphoenolpyruvate; PPIX = protoporphyrinogen IX; TCA = tricarboxylic acid.

Re-analysis of the *P. anserina* CLPP-null metabolome profile at day 5 of culture (Table S1) revealed that the ornithine decrease was not significant, due to an extremely high statistical outlier among the wildtype values, with the corrected fold-change at 0.79 (p=0.14). Among all amino acids, arginine showed the strongest reduction in fold-change (FC=0.73; p=0.005), followed by glycine

Preprints (www.preprints.org) | NOT PEER-REVIEWED | Posted: 19 January 2024 doi:10.20944/preprints202401.1423.v1

(FC=0.74; p=0.001), histidine (FC=0.74; p=0.004) and proline (FC=0.79; p=0.006), as shown in Figure 3. While the Gly decrease can be explained by the increased δALA production, the Arg / His / Pro decreases remain to be understood. The low levels of 2PG / 3PG / PEP together with the accumulation of hexose-6-phosphate and hexose-1,6-bisphosphate suggest altered glycolytic flux. In the TCA cycle, the lowered levels of fumarate contrasted with the elevated levels of citrate / isocitrate / aconitate. All findings can be explained by maximized heme synthesis within the following scenario: Decreased fumarate and Gly levels are due to increased sequestration of succinyl-CoA and glycine for δALA biosynthesis, reflecting low TCA cycle activity with resulting bioenergetics deficits (low NADPH and ATP). Cellular efforts to replenish succinyl-CoA would catabolize Thr and Hse and would generate alpha-ketoglutarate by breakdown of Arg / His / Pro (see Figure 2). Other signals would accelerate glycolytic breakdown to provide acetyl-CoA, in parallel to Asn catabolism to oxaloacetate, for maximized production of citrate / aconitate / isocitrate, which accumulate before the step of alpha-ketoglutarate / succinyl-CoA conversion to δALA.

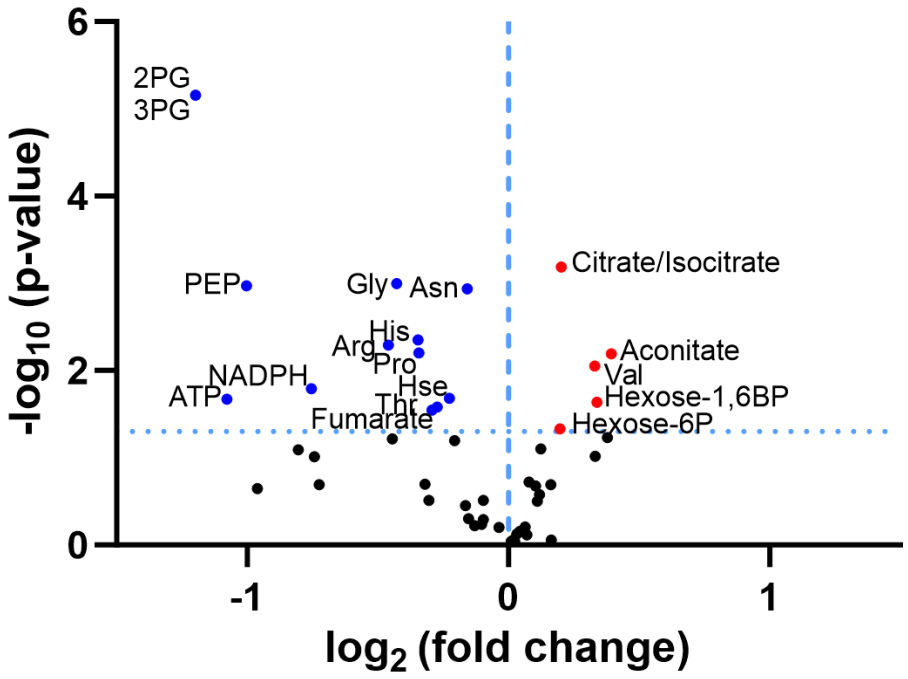

Figure 3. Volcano plot analysis of *P. anserina* CLPP-null metabolome data at day 5 of culture, previously reported in [55]. The significance threshold is represented as horizontal dotted line. Blue dots illustrate significant downregulations, red dots significant upregulations. Arg = arginine; Asn = asparagine; ATP = adenosine-trisphosphate; Gly = glycine; His = histidine; Hexose-6P = hexose-6-phosphate; Hexose-1,6BP = hexose-1,6-bisphosphate; Hse = homoserine; NADPH = Nicotinamide adenine dinucleotide phosphate; 2PG = 2-phosphoglycerate; 3PG = 3-phosphoglycerate; PEP = phosphoenolpyruvate; Pro = proline; Thr = threonine; Val = valine.

New proteome profiling data of Δ*PaClpP* by label-free mass-spectrometry quantified the most abundant 1308 proteins (Table S2). The findings confirmed the absence of CLPP (UniProt-ID B2B591) but failed to detect the known CLPX homolog (B2B254 or A0A090CGT2), probably due to technical issues. The data revealed elevated levels for homologs of mitochondrial OTC (A0A090CVB0, 2.04-fold, p=0.02) and mitochondrial OAT (B2AXK5, 1.75-fold, p=0.09). In contrast, homologs of GLDC, GOT2, BCAT2, NFS1, and SHMT2 as putative CLPP-interactors were not found among these abundant dysregulated proteins. Increased OAT abundance has not been observed in ClpP-null bacteria, but is consistent in the eukaryotes *P. anserina*, mouse, and human [3], so it might be a consequence of the heme biosynthesis switch from the Beale C5 pathway in bacteria to the Shemin

Preprints (www.preprints.org) | NOT PEER-REVIEWED | Posted: 19 January 2024 doi:10.20944/preprints202401.1423.v1

C4 pathway in eukaryotes. Interestingly, the volcano plot analysis of this proteome profile (Figure 4) reveals four massive upregulations in response to the absence of CLPP, concerning an S-adenosyl-methionine-(SAM)-dependent O-methyltransferase (B2ADP0, homologous to yeast Tae1), homologs of the mitoribosomal large subunit proteins uL30m (B2B147, ferredoxin-like) and bL33 (B2ARQ6, zinc-binding), and a heterokaryon incompatibility protein (B2AMZ4).

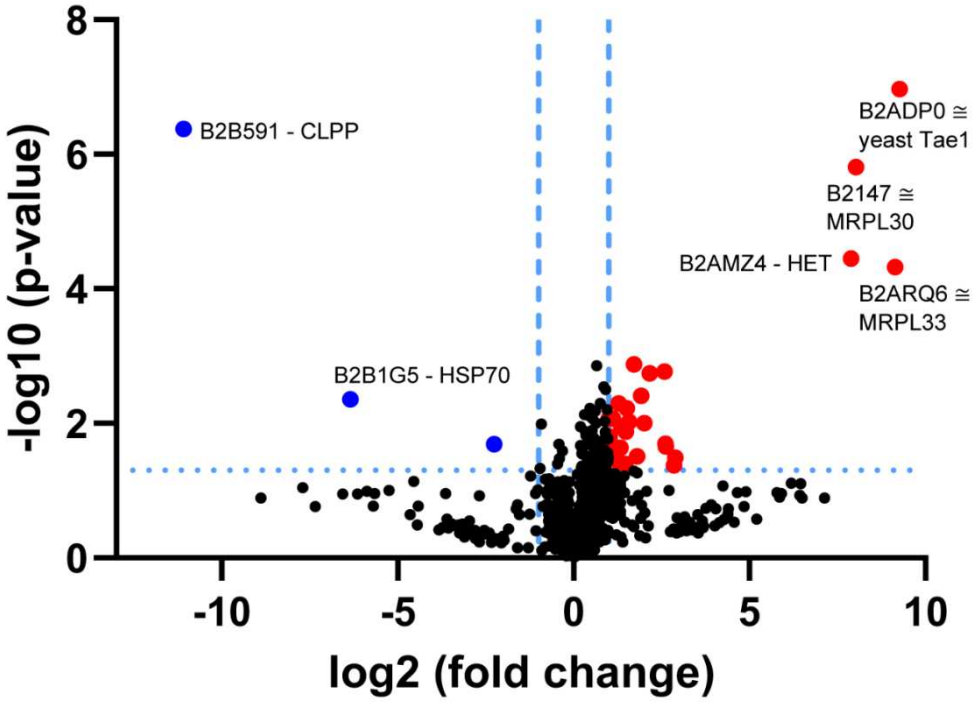

Figure 4. Volcano plot analysis of *P. anserina* CLPP-null proteome profile at 8 days of culture. Blue dots illustrate significant ($p<0.05$) downregulations, and red dots significant upregulations. Symbols beyond the uninterrupted threshold lines in volcano shape passed additional multiple testing correction and therefore have maximal stringency and credibility. HSP70 = heat shock protein 70 kDa; Tae1 = yeast alpha N-terminal protein methyltransferase 1; MRPL30 = mitoribosomal large subunit protein uL30m; MRPL33 = mitoribosomal large subunit proteins bL33; HET = heterokaryon incompatibility protein.

The dysregulation of SAM-dependent methyltransferases is substantiated further by the significant upregulation of B2B823 and B2AQK9 (Figure 4 and green background in Table S2). If CLPX is involved not only in PLP/vitamin-B6 binding to enzymes but also in cobalamin/vitamin-B12 binding to enzymes, then this general accumulation of several SAM-dependent enzymes might be due to altered recycling of SAM by methionine synthase [9]. A SAM-dependent methyltransferase known in the mammalian metabolism of ornithine/arginine is GAMT (Figure 2). More importantly, SAM-dependent methyltransferases mediate the maturation of tRNAs, ribosomes, and translation in mitochondria [63], in particular a late-stage assembly checkpoint of the mitoribosomal large subunit (LSU) [64]. The massive accumulation of two mitoribosomal LSU subunits in CLPP-null *P. anserina* is further emphasized by milder but significant accumulations of proteins B2AWM1, B2ARN9, B2A8Y5, B2B564, B2B654, B2APU3, B2B826, B2AVL5, B2ABP6, B2A9D6 (Figure 4 and yellow background in Table S2) as components of the mitoribosomal LSU and the translation elongation pathway. These findings are consistent with the selective impact of CLPP absence on two mitoribosomal LSU intermediate assemblies in mouse tissues, which was recently observed [18]. Nothing is known about the cellular functions of the heterokaryon incompatibility protein B2AMZ4.

Further pathway dysregulations in Table S2 include (i) the respiratory chain complexes I / IV with B2B1C3, B2B7U7, A0A090CEV3, B2AR53, B2AWS7, B2AT34, B2AR06, B2B5R1, P20682, B2AYP8 (orange background), (ii) the molecular chaperones with A0A090CCG8 and B2B1G5 (lilac

 doi:10.20944/preprints202401.1423.v1

background), (iii) two acetyl-CoA and acyl-CoA synthases with A0A090D6B4 and B2B6I3 (light red background), as well as (iv) the putative prolyl-3-hydroxylase-2 A0A090CDR3 that would modulate the UPR^{mt} via ATF4 (blue background) [65].

Overall, this proteome profile of CLPP-null *P. anserina* showed selective dysregulations of mitoribosomal LSU and respiratory complex I / IV factors, as well as molecular chaperones just like the CLPP-null mouse proteome profiles [18,39].

3.2. Discovery survey of cognate amino acid levels in CLPP-null mouse cerebellum:

To further elucidate by mouse metabolomics whether classical amino-acid levels and their catabolism via gluconeogenesis or ketogenesis show similar changes as in *P. anserina*, a first-tier basal metabolic screen was performed in CLPP-null cerebellum, a tissue preferentially affected by the progressive ataxia of PRLTS3 patients. We chose this central nervous tissue also because the blood-brain-barrier stabilizes amino-acid homeostasis counteracting the variance of food uptake. This first-tier survey was performed by a commercial service and documented significantly lowered levels for many amino acids (Ser, Arg, His, Trp, Asp, Phe, Met) including arginine, while ornithine levels were too low for detection in this approach (Figure 5 and Table S3). The prominent reduction in Ser levels is probably correlated with the consistent accumulation of SHMT2 protein in mammalian CLPP-null cells (see Figure 2 in [39]), which consumes Ser to resupply Gly levels that are depleted by δALA biosynthesis. In parallel, SHMT2 would transfer one carbon to 5,10-methylenetetrahydrofolate (5,10-MTHF) as a key metabolite for the folate cycle and the methionine cycle, which generate S-adenosyl-methionine as cofactor for methyltransferases. Indeed, the mitochondrial bifunctional methylenetetrahydrofolate dehydrogenase/cyclohydrolase MTHFD2 as the enzyme immediately downstream from Ser-Gly conversion showed 3-fold elevated abundance in CLPP-null mouse brain proteome profiles (see Table S3 in [39]).

The only amino acid with abnormally high levels was alanine, which is generated from pyruvate via transamination, when the enzyme GPT releases the amino group from glutamate to generate alpha-ketoglutarate (see Figure 2), as a source of succinyl-CoA for subsequent δALA biosynthesis. Again, TCA cycle activity appeared affected by CLPP-null status, given that the intermediate metabolites fumarate, succinate, and malate were accumulated and acetyl-CoA as a substrate of TCA consumption showed low levels (Figure 5 and Table S3). Overall, the data indicate that low levels of many amino acids contrast with high levels of many keto-acids, so in mouse, the PLP-dependent transaminations may be affected subtly in a general manner.

Preprints (www.preprints.org) | NOT PEER-REVIEWED | Posted: 19 January 2024 doi:10.20944/preprints202401.1423.v1

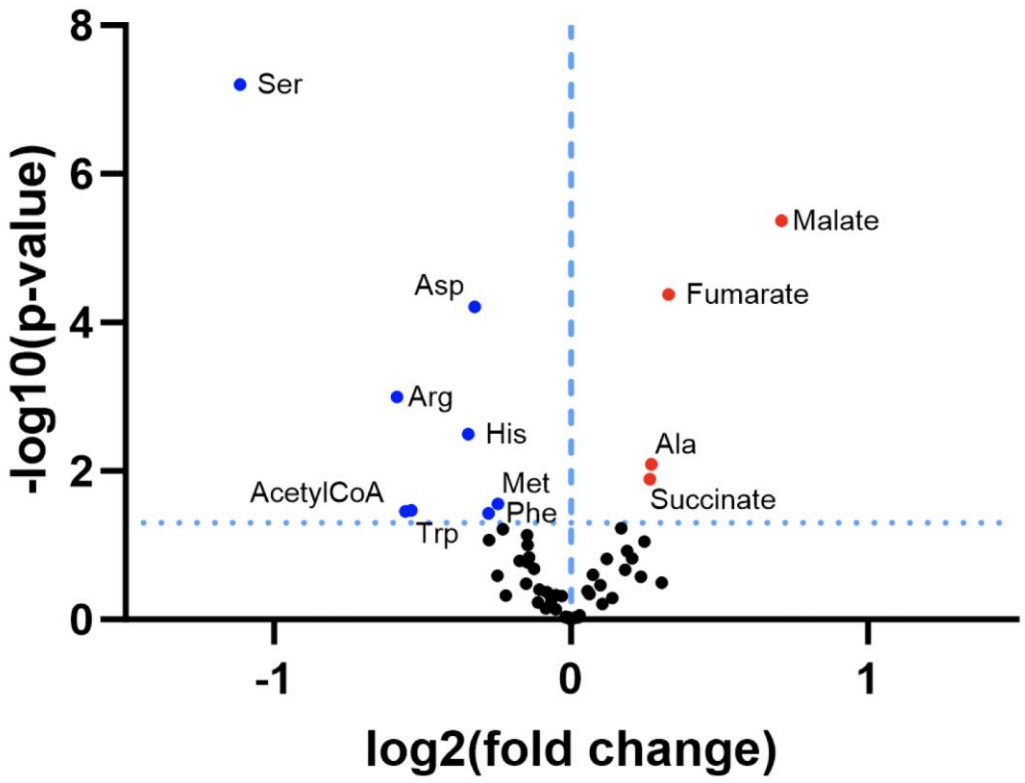

Figure 5. Volcano plot analysis of adult *CLPP*-null cerebellum metabolome. The significance threshold is represented as a dotted line. Blue dots illustrate significant ($p<0.05$) downregulations, and red dots significant upregulations.

3.3. Confirmatory survey with selected non-cognate amino acids in CLPP-null mouse cerebellum:

To re-assess the effects with additional samples in an independent academic lab, and to elucidate how non-proteinogenic amino acids are affected in CLPP-null cerebellum, a second-tier metabolomic validation study was added. This approach confirmed low Arg and Ser levels, as well as high Ala amounts with significance after multiple testing correction, and low Gln, acetyl-Gln, and Asp versus high Pro levels with nominal significance (Table S4). These findings are compatible with a scenario where the increased δALA biosynthesis from Gly and succinyl-CoA is compensated by Ser and alpha-ketoglutarate. The production of the latter reduces Gln / acetyl-Gln stores while increasing Ala. In addition, accelerated breakdown of Arg leads to more Pro. Asp is consumed to replenish fumarate (see Figure 2).

In addition, reduced steady-state levels were found for the non-canonical amino acid derivatives citrulline (Cit and its derivatives Orn and Arg share amino groups at the alpha- and delta-carbon, see Figure 1) (FC=0.67; p=0.02) and 1-methylhistamine (1-MHis, the main catabolite of histamine, is derived from histidine that has a second amino group attached to the delta-carbon) (FC=0.83; p=0.01). Histidine was not studied in this analysis. In contrast, excess quantities were documented for the oxidized glutathione (GSSG, with a delta-amino-group) (FC=1.46; p=0.02) and the (δALA-derived) heme precursor protoporphyrin-IX (PPIX) (FC=4.70; p=4.1e-07) (Figure 6). In comparison to the 30% accumulation of alanine (Ala), the accumulation of the δALA-derived PPIX was much bigger, probably a simple reflection of the fact that there is much more Ala than δALA in any cell. Compared with the 47% reduction of serine, the 55% decrease of arginine (Arg) was stronger in this experiment, a novel observation that may suggest that δALA biosynthesis can be fuelled more by Arg/Orn than by Gly/Ser in CLPP-null mouse cerebellum. Furthermore, non-proteinogenic Cit showed a stronger decrease than all other classical amino acids (Figure 6). In contrast, the basal polyamine putrescine was not elevated (Table S4). Overall, these mouse data suggest that absent CLPP with excess CLPX may influence the PLP-dependent transamination more strongly at delta-carbon positions than at alpha-carbons.

Preprints (www.preprints.org) | NOT PEER-REVIEWED | Posted: 19 January 2024 doi:10.20944/preprints202401.1423.v1

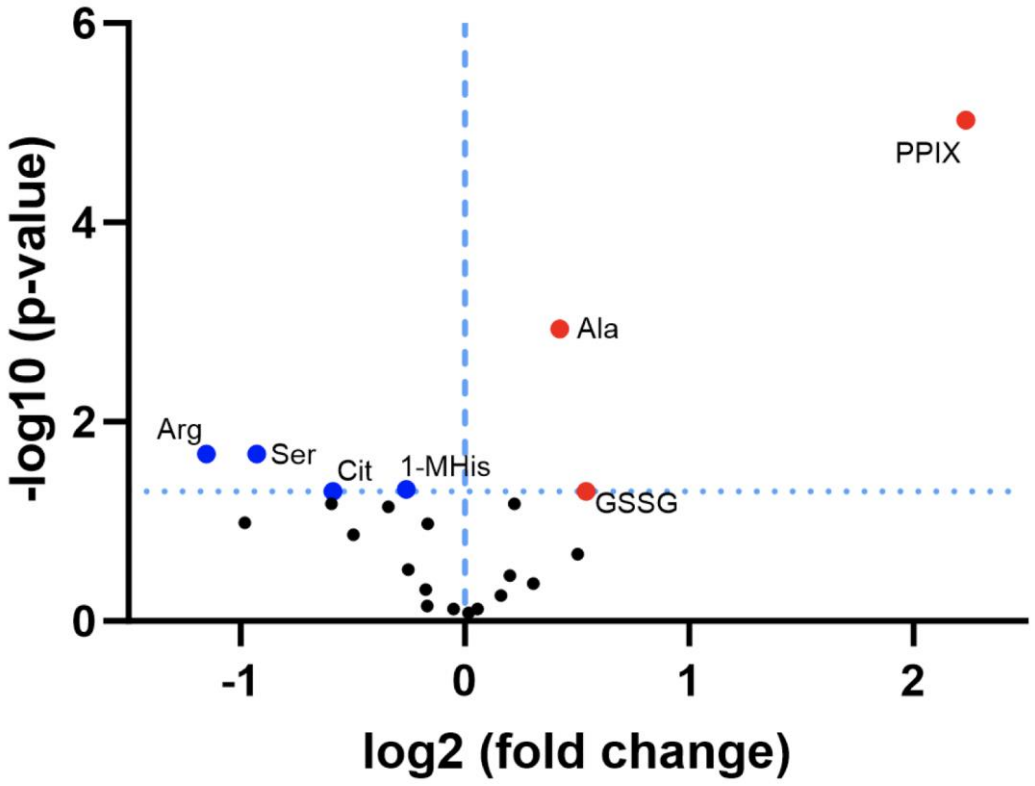

Figure 6. Volcano plot of cognate and selected non-cognate amino acids and derivatives in adult CLPP-null cerebellum. Again, the significance threshold is represented as a dotted line. Blue dots illustrate significant downregulations, and red dots significant upregulations. GSSG = oxidized glutathione; 1-MHis = 1-methylhistamine; PPIX = protoporphyrinogen IX.

4. Discussion

4.1. CLPP-absence affects amino-acid metabolism

The main novel finding of this study with consistency between mouse cerebellar tissue and P. anserina young cultures is that the absence of CLPP leads to consistent and particularly strong reductions of Arg and its related compounds Cit and His, which share a C5 core and - attached at the delta-carbon position - a guanidino-group that is converted to keto-acid or circular form. All three compounds are convertible to the metabolite alpha-ketoglutarate which is the substrate for succinyl-CoA generation within the TCA cycle and are thus presumably channeled into the excess biosynthesis of δALA.

We have to consider that CLPP absence is known to result in a several-fold excess of CLPX, with consequent heme biosynthesis activation via PLP-binding to ALAS, which utilizes succinyl-CoA and glycine. Indeed, if succinyl-CoA is not broken down to succinate / CoA / GTP within the TCA cycle, but instead used to build δALA within heme biosynthesis, then the GTP reduction to 21% observed in Table S1 can be explained with ease. However, such a chronic sequestration of a metabolite from the TCA cycle would hamper the cellular bioenergetics, and indeed the significant reduction of ATP levels in the P. anserina metabolome reflects a mitochondrial bioenergetic deficit. The C4 compound succinyl-CoA could be repleted more directly by the breakdown of amino acids with a C4 core chain, namely Thr, Hse, Val, Met (see Figure 2), but this option is only partially supported by our observations. As a stronger contribution, an apparently more indirect repletion within the TCA cycle from the C5 chain compound alpha-ketoglutarate, and externally via Glu by breakdown of C5-chain amino acids Orn, Arg, Cit is apparent (see Figure 1 and 2). However, the levels of Glu/Gln are not altered strongly, presumably because they are replenished from His. It is important to note here that an accumulation of P5CS/ALDH18A1 enzyme was documented consistently in mammalian CLPP-null proteome profiles (2-fold in brain, see Table S3 in [39]; 3-fold in testis at P21, see Table S1 in [45]),

 doi:10.20944/preprints202401.1423.v1

indicating increased activity to produce G5SA from Glu as well as from Orn. Therefore, it is conceivable that increased G5SA generation on the one hand from Orn, Arg, Cit, and on the other hand from Glu can be channeled directly into δALA biosynthesis without detour conversions to Glu / alpha-ketoglutarate / succinyl-CoA. This might occur within a single step, if OAT after PLP-activation by excessive CLPX abundance undergoes a gain of a GSA 1,5-aminomutase function. For a metabolic conversion of G5SA to δALA an enzyme would have to bind to the carboxy-group and then reposition the amino group from the alpha-carbon to the delta-carbon, and the keto-group from the delta-carbon to the gamma-carbon (see Figure 1). In view of the sequence homology between the bacterial GSA 2,1-aminomutase HemL and mitochondrial OAT, together with their structural and mechanistic similarities [66], this seems conceivable. Thus, a remainder of the archaeal C5-pathway of ALA-biosynthesis might be activated to coexist with the eukaryotic C4-pathway in cells with maximized heme biosynthesis due to CLPX excess. Of course, such direct conversion of G5SA to δALA via OAT together with the more indirect conversion of G5SA via Glu / alpha-ketoglutarate / succinyl-CoA to δALA would both contribute Arg to heme biosynthesis, while elevating the alanine levels. This scenario would explain the observations of 5-fold increased levels of PPIX with the concomitantly about 2-fold reduced levels of Cit, Arg (and Orn?) via the C5 pathway, plus the two-fold decrease of Gly or Ser via the C4 pathway, providing a tentative first mechanistic explanation of several metabolome findings.

These novel metabolomic findings can be explained by the accumulation of excess ornithine-delta-aminotransferase (OAT), shown in Table S2 for P. anserina, which was previously documented also for mouse tissues [18]. In P. anserina it is known that OAT is a protein-protein interactor of overexpressed WT CLPP [56], and previous work in mouse testis tissue confirmed a protein-protein association between endogenous amounts of OAT and CLPX [18]. The quaternary structure of OAT is a homohexameric ring, where each subunit is activated by PLP association. Thus, it is likely that CLPX as a monomer or homoheptameric ring unfolds the OAT ring to enable its activation by PLP. Overactive OAT would metabolize Arg-derived Orn, acting either as delta-transaminase to produce G5SA (see Figure 1) for subsequent conversion to Glu and the C4 compound succinyl-CoA, or acting first as delta-transaminase and then also as GSA 1,5-aminomutase to produce δALA directly (see Figure 1). Orn even more than Cit is a transient intermediate, usually below detection limits in mammals, but plays a crucial role at the crossroads between amino-acid metabolism, polyamine biosynthesis, urea excretion, and creatine bioenergetics (see Figure 2), therefore the regulation of its processing by OAT is probably decisive.

Thus, the CLPX excess of CLPP-null organisms would overactivate ALAS and OAT, jointly causing lower arginine levels. It is important to note that arginine contains 4 amino groups per molecule, so in mammals it represents the main nitrogen storage reserve for growth [67]. Body length and muscle mass depend crucially on the availability of nitrogen, taken up mainly as amino acids within proteins [68]. The levels of arginine are therefore a decisive signal in the pituitary signaling pathway to secrete growth hormone (GH) [69]. This is also the reason why arginine is used routinely by body builders as a diet "pump-supplement" [70]. The reduction of arginine to 47% in CLPP-null mouse tissues (Table S4) is, therefore, an excellent explanation for their decrease of body weight to around 50% [8], and for the low body size of PRLTS3 patients below the third percentile [36]. It is relevant to know that diet supplementation of L-arginine was successfully used to rescue the growth deficits of a patient with mitochondrial Barth syndrome where GH-unresponsiveness was observed [71]. Thus, we propose that supplementation of excess arginine in the diet of PRLTS3 patients will partially prevent and revert their growth deficit. In contrast to this mammalian phenotype, growth is not affected in the P. anserina ClpP-null mutant [54], probably because nitrogen is readily available in cells (e.g., in the chitin of the cell wall) and in nature on the substrate (herbivorous dung) on in which this fungus grows. The nitrogen storage role of arginine is therefore not critical in this fungus.

Of course, the question arises if (i) the increased heme biosynthesis, (ii) TCA cycle impairment due to succinyl-CoA depletion with consequent reduction of GTP and acetyl-CoA, and (iii) Arg/Cit/His-decrease in their combination are also relevant for the impact of CLPP-antagonist drugs on the growth of bacteria and cancer cells. It also remains to be explored if the effect of CLPXP-

 doi:10.20944/preprints202401.1423.v1

modulated, PLP-dependent amino-acid metabolism has an overall impact on the urea cycle and organismic nitrogen utilization versus release.

The deficit of glycine in the metabolic profile of CLPP-null P. anserina might simply reflect the excessive δALA synthesis from Gly and the C4 substrate succinyl-CoA (see summary scheme in Figure 7 below). In mitochondria, Gly is degraded to amino groups and CO_2 by the PLP-dependent enzyme GLDC and is converted to Ser by the PLP-dependent enzyme SHMT2, both of which were identified as CLPP-interactors [56]. Thus, also the prominent Ser reduction in CLPP-null mouse cerebellum, together with the elevated abundance of SHMT2 and MTHFD2, might reflect an excessive activity of PLP-activated SHMT2.

In agreement with the concept that the archaeal/bacterial C5 pathway of δALA biosynthesis is not conserved to mammals because an ortholog of the glutamyl-tRNA-reductase HemA does not exist, there was only a statistical trend to a 20% increased amount for the GltX ortholog EARS2 as mitochondrial glutamyl-tRNA-synthase in the CLPP-null mice brain (see Table S3 in [39]). However, it is interesting to note that the abundance of the mitochondrial glutaminyl-tRNA-synthase component GATC showed even stronger significant elevation (7.1-fold) than ALAS1 (3.9-fold) in CLPP-null mouse brain proteome profiles (see Table S3 in [39]), suggesting that tRNA-Gln instead of tRNA-Glu might be recruited as C5 source for heme production in PRLTS3 (compare Figure 1).

The reduction of His was less prominent than the reduction of Arg in the three surveys performed but had a stronger fold-change than the remaining proteinogenic amino acids. Lowered His levels would have an impact on metal ion chelation (e.g., Fe^{2+} binding to heme via His, which serves generally as ligand within metalloproteins), heavy metal stress sensing (histidine kinases), scavenging of reactive oxygen and nitrogen species, and histaminergic signaling. The degradation of His to Glu is not modulated by PLP, so its decreased levels can be only explained by the increased flux to replete alpha-ketoglutarate and succinyl-CoA in the TCA cycle. However, PLP-dependence exists for the conversion of His to histamine by the enzyme histidine decarboxylase. The notion of deficient availability of histamine is supported by the low levels of 1-methylhistamine in the metabolome profile of CLPP-null cerebellum. Histamine acts as a signaling molecule and is stored e.g. in mast cells below body surfaces. A lack of histamine would restrict itchy feelings and inflammatory responses upon bacterial infection of the skin. The His deficit and the likely histamine deficit therefore explain the resistance to ulcerative dermatitis that was observed for CLPP-null mice with C57BL/6 genetic background [8,50].

Preprints (www.preprints.org) | NOT PEER-REVIEWED | Posted: 19 January 2024 doi:10.20944/preprints202401.1423.v1

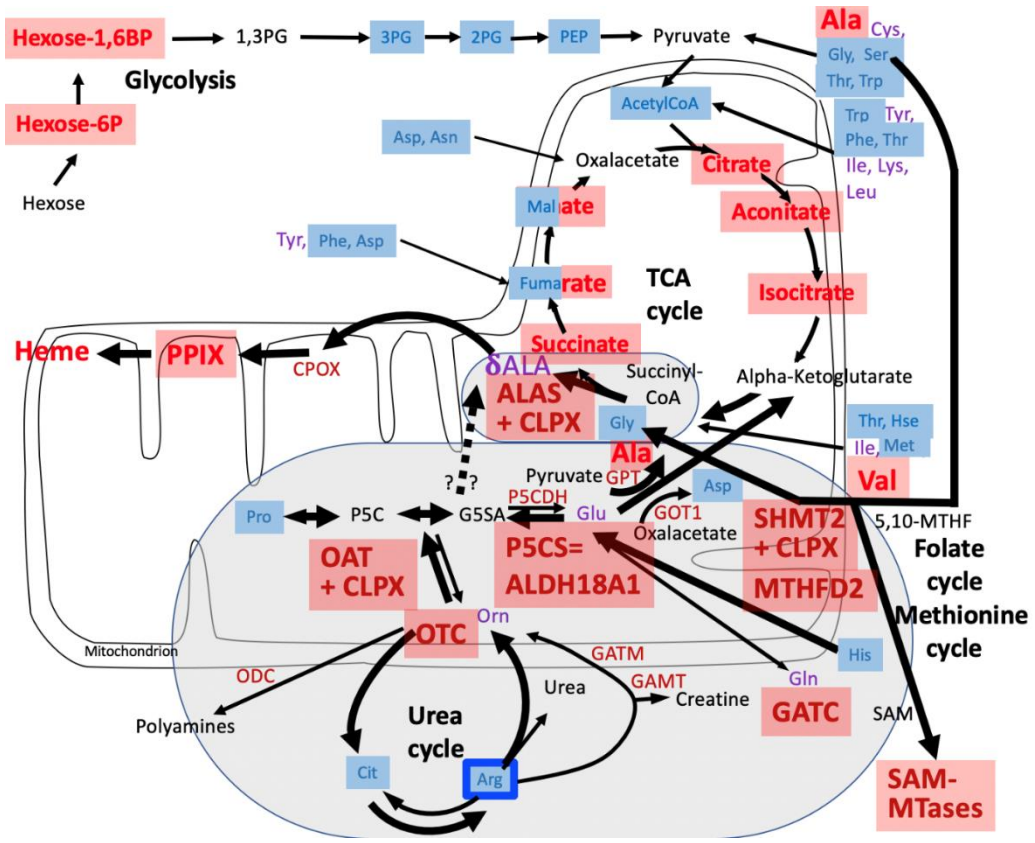

Figure 7. Summary of *P. anserina* culture and mouse cerebellum observations, how the breakdown of amino acids for consumption in the mitochondrial TCA cycle, and extra-mitochondrial metabolite flux from urea cycle and glycolysis towards heme biosynthesis is changed in CLPP-null cells, compared to the WT scenario in Figure 2. As in Figure 2, the Shemin pathway - as primarily responsible for heme biosynthesis - is again highlighted in an ellipse with a gray background. In Figure 6 an additional gray ellipse emphasizes the recruitment of additional metabolites when excessive heme biosynthesis occurs upon CLPP absence and CLPX excess. Broader arrows suggest an increased metabolite flux in CLPP-null eukaryotes. Blue background and smaller letter font indicate downregulation, red background and bigger letter font illustrate upregulations; bicolor background reflects different regulations in *P. anserina* versus mouse. The complete consistency of arginine reduction is highlighted by a blue frame. Enzymes are shown in auburn (red-brown) letters: ALAS = delta-amino levulinic acid synthase; CLPX = caseinolytic mitochondrial matrix peptidase chaperone subunit X; CPOX = coproporphyrinogen oxidase; GAMT = guanidinoacetate N-methyltransferase; GATC = glutamyl-tRNA amidotransferase subunit C in mitochondria; GATM = glycine amidinotransferase; GOT1 = glutamic-oxaloacetic transaminase 1; GPT = glutamic-pyruvic transaminase; MTHFD2 = bifunctional methylene-tetrahydrofolate dehydrogenase in mitochondria; OAT = ornithine delta-aminotransferase; ODC = ornithine decarboxylase; OTC = ornithine transcarbamylase; P5CDH = pyrroline-5-carboxylate dehydrogenase; P5CS = pyrroline-5-carboxylate synthetase = ALDH18A1 = aldehyde dehydrogenase 18 family member A1; SAM-MTases = S-adenosyl-methionine-dependent methyltransferases; SHMT2 = serine-hydroxymethyltransferase 2 in mitochondria. Amino acids are shown in purple letters: Ala = alanine; δALA = delta-amino levulinic acid; Arg = arginine; Asn = asparagine; Asp = aspartate; Cit = citrulline; Cys = cysteine; Gln = glutamine; Glu = glutamine; Gly = glycine; His = histidine; Hse = homoserine; Ile = isoleucine; Leu = leucine; Lys = lysine; Met = methionine; Orn = ornithine; Phe = phenylalanine; Pro = proline; Ser = serine; Thr = threonine; Trp = tryptophan; Tyr = tyrosine; Val = valine. Other metabolites are shown in black letters: 5,10-MTHF = 5,10-methylene-tetrahydrofolate; CoA = coenzyme A; Hexose-6P = hexose-6-phosphate; Hexose-1,6BP = hexose-1,6-bisphosphate; 1,3PG = 1,3-bisphospho-glycerate; 2PG = 2-phosphoglycerate; 3PG = 3-phosphoglycerate; PEP = phosphoenolpyruvate; PPIX = protoporphyrinogen IX; SAM = S-adenosyl-methionine; TCA = tricarboxylic acid.

 doi:10.20944/preprints202401.1423.v1

4.2. CLPP-absence affects mitoribosomal LSU and its rRNA/tRNA$^{Val/Phe}$

A second novel finding of this study in the *P. anserina* CLPP-null proteome profile is the strong selective accumulation of two components of the mitoribosomal LSU. Similarly, in CLPP-null mice, CLPX was shown to have a selective effect on mitoribosomal LSU components [18]. Both in *P. anserina* and in mouse CLPP-null organisms, the affected proteins are constituents of the LSU central protuberance, which contains the 5S rRNA or tRNA$^{Val/Phe}$ which associates with LSU 16S rRNA [72].

Two LSU proteins showed massive upregulation: B2B147 has a ferredoxin-like β-α-β-α-β-fold core structure, and B2ARQ6 has a zinc-binding domain, so both factors potentially associate with heavy metals, and recent mouse analyses documented several heavy metals to accumulate in CLPP-null tissue [18].

Additional ribonucleoproteins were also significantly accumulated with modest fold-change, but they appear to represent a very selective pattern acting on LSU components:

B2AVL5 (L31 family) is homologous to a bacterial ribosomal LSU component that associates with 5S rRNA and is lost from mitoribosomes in mammals [72].

B2ARN9 (mL41 family) is a mitochondria-specific protein that compensates for lost rRNA in the mitoribosomal LSU [72].

B2A8Y5 (mL53 family) is part of the glutaredoxin superfamily, also a mitochondria-specific protein that connects the L7/L12 stalk to the central protuberance of the mitoribosome next to uL30 [72].

B2B826 (ribosomal protein P1/P2) is localized in the L7/L12 stalk and has important roles in the elongation step of protein synthesis, as shown for cytosolic ribosomes.

B2ABP6 is the synthetase for tRNA^{Val}, which replaced 5S rRNA in the LSU central protuberance during eukaryotic evolution.

B2AWM1 (homolog of eIF6) is required for LSU biogenesis of 60S subunits; its disassociation permits binding to SSU and formation of the translation initiation complex [73]. Its binding occurs near the L7/L12 stalk at uL3/uL11/uL14/uL16/L23/L24 in competition with translation elongation factor G, mouse GFM1/GFM2 [74–76]. It belongs to the pentein superfamily of peptidylarginine-deiminases (PADI), with succinylarginine-dehydrolase, dimethylarginine dimethylaminohydrolase and arginine-glycine-amidinotransferase (AGAT/GATM, see Figure 2), and it can be blocked by the protein-arginine-methyltransferase antagonist drug eIFsixty-4 [77]. While it is unclear if it retains enzymatic activity, presumably it also binds to a peptidylarginine moiety. Therefore, the dysregulation of this factor provides a clear link with the arginine deficit in CLPP-null organisms.

B2B654 (NOP10 family) is a subunit of the H/ACA ribonucleoprotein complex responsible for the pseudouridylation of rRNA, tRNA, and snoRNA [78,79].

B2APU3 (GAR1 family, metallophosphatase DUF2433 family) is also a subunit of the H/ACA ribonucleoprotein complex responsible for the pseudouridylation of rRNA, tRNA, and snoRNA [78,79].

While all the above factors target selectively the mitoribosomal LSU and its rRNA or tRNA^{Val}, the subsequent proteins are thought to act on mRNAs or are poorly understood ribonucleoproteins:

B2A9D6 (Small nuclear ribonucleoprotein G) with Lsm7/SmG-like domain. It assembles with other Sm-proteins into a hetero-heptameric ring around the Sm site of the 2,2,7-trimethyl guanosine (m3G) capped U1, U2, U4, and U5 snRNAs (Sm snRNAs) forming the core of the snRNP particle. The snRNP particle, in turn, assembles with other components onto the pre-mRNA to form the spliceosome which is responsible for the excision of introns and the ligation of exons.

B2B564 contains a DNA/RNA-binding SAP domain at the N-terminus.

Thus, the mitoribosomal translation fidelity and elongation problems previously reported in CLPP-null mice do not seem caused only by lacking GTP or deficient hypusine, entailing the accumulation of translation elongation proteins and ribosome recycling proteins, but rather are reflected by specific alterations of mitoribosomal LSU rRNA/tRNA^{Val} factors. Whether abnormal methylation of rRNA or peptidylarginine plays a role, remains unclear.

What scenario might link CLPXP delta-amino-acid-preference with the mitoribosomal translation pathology? There is no established link between PLP and pseudouridylation or SAM-

 doi:10.20944/preprints202401.1423.v1

dependent methylation in mitochondrial RNA processing. However, it is conceivable that the generation of polypeptide chains in the ribosome might have a small error rate leading to bond formation between the polypeptide carboxy-terminus at the P-site, and the delta amino group instead of the alpha amino group of the subsequent amino-acid-tRNA at the A-site. Such misincorporation problems would lead to steric problems in the nascent peptide exit channel of the LSU, and it might be a function of CLPX to recognize such bonds, and the crucial role of CLPP to degrade such abnormal polypeptides that would be marked with a C-terminal alanine-threonine-tail before release from the translation machinery. Such translation fidelity issues would arise more frequently during cell stress periods [80]. As an alternative link, the alteration of mitochondrial C1 metabolism may lead to abnormal methylation during RNA maturation, triggering misassembly of RNA with its processing and translation proteins, and thus leading to UPR^{mt}.

4.3. CLPP-absence affects SAM-dependent methyltransferases

A third novel finding of this study in the *P. anserina* CLPP-null proteome profile is the massive accumulation of the SAM-dependent O-methyltransferase B2ADP0, and the modest significant upregulations of the SAM-dependent methyltransferase-7B-like B2B823 and the SAM-dependent O-methyltransferase B2AQK9. The upstream reason for this SAM-centered pathology might be explained by altered SAM regeneration in *P. anserina*. At least in mammals, the SAM cycle depends on the cofactor cobalamin whose archaeal/bacterial biosynthesis depends on δALA availability [9], and the association of cobalamin with the enzyme methionine synthase might be modulated by CLPX similar to PLP-ALAS association. As an additional or alternative explanation, SAM-MTases may have abnormal activity due to the changes in mitochondrial C1 metabolism downstream from excess SHMT2 and MTHFD2. What would be the downstream consequences of these dysregulations? Within the superfamily of SAM-dependent methyltransferases, the most abundant and best-studied class A is defined by a partial (βα)-6 barrel structure, associates with a FeS-cluster, and acts in the processing of rRNAs and tRNAs [81]. Therefore, the strong accumulation of mitoribosomal proteins B2B147 and B2ARQ6 might be due to abnormal LSU rRNA methylation by B2ADP0, suggesting a massively abnormal pathway in the maturation of the large ribosomal subunit from the CLPP-null *P. anserina* strain. B2ADP0 contains a winged-helix-DNA-binding domain, homologous to the arginine repressor, so the dysregulation of this factor could also relate to the ornithine metabolism anomaly.

Interestingly, very close homologs of B2ADP0 according to the STRING webtool in the fungus *Aspergillus nidulans* are the enzymes asqN and asqD, which mediate steps in the biosynthesis of aspoquinolone as terpenoid mycotoxin, subsequent to the nonribosomal peptide synthetase asqK. The close homologs in the fungus *Neurospora crassa* include e.g. sterigmatocystin 8-O-methyltransferase, enzymes that are also key to the biosynthesis of the polyketide mycotoxins. These findings raise the possibility that *P. anserina* CLPP and CLPX modulate bonds between non-classical amino acids in the production of cyclic venoms as well as signaling molecules. In the yeast species *Saccharomyces cerevisiae* and *Schizosaccharomyces pombe*, the best homology is with Tae1 as alpha-N-methyltransferase that methylates the N-terminal motif [Ala/Pro/Ser]-Pro-Lys of target proteins when the initiator Met has been cleaved. Tae1 modifies several ribosomal proteins [82]. An additional possibility is therefore that CLPXP via SAM-dependent methylation modulates the N-terminal processing of target proteins. However, the cytosolic enzymes ASMT, NTMT1, and NTMT2 as the closest sequence-homologs of B2ADP0 in mice did not show a significant dysregulation in CLPP-null mouse proteome profiles. Instead, prominently and consistently elevated abundance in several CLPP-null mouse tissues was observed for the mitochondrial S-adenosyl-methionine-dependent N-methyltransferase TRMT10C (=MRPP1) (3.1-fold in brain, see Table S3 from [39]; 2-fold in testis at P17 and P21, see Table S1 from [45]), which acts together with two more components of the RNAse-P complex, in order to excise tRNAs from the mitochondrial polycistronic transcript, and to ensure their correct folding [83,84]. Its function requires interaction with the RNAse-P endonuclease component PRORP (=MRPP3), where mutations are known to also cause a Perrault syndrome phenotype [41]. Any problems in the maturation of diverse tRNAs due to dysfunction of TRMT10C or PRORP would of course impair the assembly of the mitoribosomal LSU central protuberance

Preprints (www.preprints.org) | NOT PEER-REVIEWED | Posted: 19 January 2024 doi:10.20944/preprints202401.1423.v1

around the $tRNA^{Val/Phe}$, and even in successfully assembled mitoribosomes the translation efficiency would be reduced.

Previous *P. anserina* work has already demonstrated the accumulation of another mitochondrial SAM-dependent methyltransferase (UniProt-ID Q9HGR1) during the aging process [85], and the protective effect of its overexpression on lifespan [86], while its deletion resulted in vulnerability towards metal-triggered oxidative stress [87–89]. Our current data may correlate the accumulation of SAM-dependent O-methyltransferase B2ADP0 as the main proteome finding with the extended lifespan observed for the CLPP-null strain. It should be mentioned that the superfamily of methyltransferases contains spermidine synthase as its ancient prototype, so it is also possible that the methylation targets a polyamine rather than a ribonucleoprotein complex. Polyamines are crucial for growth, healthy aging, and lifespan [90].

4.4. CLPP-absence affects molecular chaperones and the UPR^{mt}

A fourth novel finding of this study in the *P. anserina* CLPP-null proteome profile is the modest accumulation of molecular chaperones and a potential UPR^{mt} regulator.

A0A090CCG8 is a BAG-domain-containing protein. Bcl2-associated athanogene (BAG) family proteins can interact with the HSP70 proteins and regulate them, exerting an anti-apoptotic effect. Therefore, its accumulation may reflect the UPR^{mt} via molecular chaperone upregulation. However, it is interesting to note that STRING homology searches in *Neurospora crassa*, *Caenorhabditis elegans*, *Drosophila melanogaster*, *Danio rero*, *Xenopus laevis*, *Mus musculus and Homo sapiens* find low similarity between A0A090CCG8 and the lysosomal cobalamin transporter LMBRD1, an interesting observation given the cobalt accumulation documented in CLPP-null mouse tissue [18]. Cobalamin production in archaea/bacteria depends on the availability of corrin rings that are produced from δALA. Cobalamin is an essential cofactor for mitochondrial methylmalonyl-CoA mutase, and for methionine synthase in the re-methylation of homocysteine to methionine with concurrent SAM regeneration, which is crucial for all S-adenosylmethionine-dependent methylation reactions [91]. Of course, cobalamine binding to mammalian enzymes might also be modulated by CLPX, like PLP binding to ALAS and OAT.

B2B1G5 is homologous to DnaK and belongs to the HSP70 family. Its accumulation suggests that the altered unfoldase/disaggregase role of CLPX results in a compensatory upregulation and/or delayed turnover of the HSP70 chaperone system, attempting to correct misassembled protein complexes.

This is in line with the significant accumulation of A0A090CDR3 as a protein with sequence homology to prolyl-3-hydroxylase-2. In human cell culture, the prolyl-hydroxylase domain containing oxygen sensor PHD3 modulates UPR^{mt} via the oxygen-dependent transcription factor ATF4 [65]. Thus, it is conceivable that the abnormal mitochondrial translation and membrane insertion of respiratory chain core proteins will trigger UPR^{mt} and ATF4 activation together with dysregulation of its upstream prolyl-3-hydroxylase regulator.

In CLPP-null mouse tissue, accumulations of HSP70 chaperones and co-chaperones are also prominent [18,39], and abnormal mitochondrial morphology with cristae disconnection from inner membranes was shown previously by electron microscopy [8].

4.5. CLPP-absence affects the respiratory chain

A fifth novel finding of this study in the *P. anserina* CLPP-null proteome profile is the modest accumulation of coherent respiratory complex-IV components, together with the significant minor accumulation of dispersed complex-I factors.

Regarding complex-IV:

B2B1C3 is homologous to the NADH-ubiquinone reductase complex 1 MLRQ subunit (NDUFA4=COXFA4), an assembly factor and stress-adaptor within the cytochrome c oxidase (CIV) complex [92–96].

B2B7U7 is homologous to the cytochrome c oxidase subunit VII (COX7A), another assembly factor in close cooperation with NDUFA4, which permits integration of mt-CO3 and completion of

 doi:10.20944/preprints202401.1423.v1

complex-IV [97]. Upon formation of respiratory supercomplexes, it is crucial for the interaction between complex-IV and complex-I [98].

P20682 is the mitochondrially encoded cytochrome c oxidase subunit 2 (COX2), contains the dinuclear copper A center, and enters the complex-IV assembly before COX7A and NDUFA4 act [97]. This might be a specific site of pathology given that heme excess is a known consequence of CLPP-absence and might cause problems of assembly for the heme-binding COX1 with the copper-binding COX2, and downstream alterations of complex-IV completion.

Regarding complex-I:

A0A090CEV3 is the NADH-ubiquinone oxidoreductase 9.5 kDa subunit (N9IM, homologous to NDUFA3), which serves in the proximal half of the membrane arm of complex-I (P_P ND1 module) [99,100].

B2AR06 is the NADH dehydrogenase (ubiquinone) alpha subcomplex subunit 1 (NDUFA1), which is part of the proximal half of the membrane arm of complex-I (P_P ND2 module) [99,100].

B2AR53 is homologous to the NADH:ubiquinone oxidoreductase ESSS subunit (NDUFB11), which serves in the distal half of the membrane arm of complex-I (P_D ND4 module) [99,100].

B2B5R1 is the NADH dehydrogenase (ubiquinone) 1 beta subcomplex subunit 2 (NDUFB2=CI-AGGG), which is located in the distal half of the membrane arm of complex-I (P_D ND5 module) [99,100].

B2AWS7 is the NADH dehydrogenase (ubiquinone) 1 alpha subcomplex 6 subunit (homologous to NDUFA6=LYRM6), which is placed in the Q-module before the N-module is added to the assembly of complex-I [101,102].

B2AT34 is the NADH dehydrogenase (ubiquinone) 1 alpha subcomplex 2 subunit (NDUFA2=CI-B8), which is part of the N-module of complex-I [101,102].

B2AYP8 contains a domain of complex-I subunit NDUFS6, which is placed in the matrix arm of complex-I (N-module) [99,100].

Thus, the significant but minor accumulations of complex-I subunits are unspecifically distributed across all its membrane and matrix modules. Thus, these fragmentary findings probably reflect a compensatory upregulation of the complete complex-I in face of the mitochondrial dysfunction. An accumulation of complex-I subunits was not observed in CLPP-null mouse tissues [18].

5. Conclusions

Overall, it is clear from our *P. anserina* and mouse findings, which were discussed above, that CLPP absence has consistent effects throughout eukaryotic development:

(1) The consequent accumulation of CLPX with PLP cofactor not only activates the δALA production with downstream heme biosynthesis but in parallel reduces the levels of other delta amino acids such as Arg, Cit, and His. The consistent accumulation of ornithine-delta-aminotransferase (OAT) and its probable activation by CLPX-PLP is probably contributing to this effect. The halved Arg levels probably explain the growth deficit of CLPP-null mammals, so Arg supplementation of the diet might rescue the short stature and low muscle mass of PRLTS3 patients.

(2) Absent CLPP with accumulated CLPX alters proteins in the LSU central protuberance and L7/L12 stalk, which are key for the processing and integration of the $tRNA^{Val/Phe}$ as well as SSU interaction into the complete mitoribosomal assembly.

(3) Within the mitochondrial protein aggregation pathway, HSP70 accumulation is prominent.

(4) An assembly problem at the respiratory chain complex-IV heme/copper binding subunits is compatible with mouse and *P. anserina* observations.

In summary, despite differences in phenotypic consequences, there is clear consistency between CLPP-null *P. anserina* and mouse regarding dysregulated metabolites and proteome pathways. The elevated abundances of CLPX, ALAS, and OAT are among the most highly conserved findings in proteome profiles of all species studies [3], so we identify this metabolic distortion as a probably general feature of CLPP loss.

 doi:10.20944/preprints202401.1423.v1

Supplementary Materials: The following supporting information can be downloaded at the website of this paper posted on Preprints.org. Supplementary Table S1, Supplementary Table S2, Supplementary Table S3, Supplementary Table S4.

Author Contributions: Conceptualization, H.O. and G.A.; methodology, S.G., A.H. and D.M.; software, J.K.; validation, J.K., S.G., D.H., A.H., and D.M.; formal analysis, S.G., A.H., D.M. and G.A.; investigation, J.K., D.H. and D.M.; resources, J.K., S.G., A.H., H.O. and G.A.; data curation, D.M.; writing—original draft preparation, G.A.; writing—review and editing, J.K., D.H., A.H., H.O., D.M. and G.A.; visualization, J.K. and G.A.; supervision, S.G., H.O., D.M. and G.A.; project administration, G.A.; funding acquisition, H.O., D.M. and G.A.

Funding: HDO was funded by the Deutsche Forschungsgemeinschaft (DFG, German Research Foundation) – Project-ID Os75/15-2 and Project-ID 259130777 – (SFB 1177). In addition, this project was supported by Klinikum Goethe University Frankfurt/M and Max Planck Society funds.

Institutional Review Board Statement: This study was conducted according to the guidelines of the Declaration of Helsinki and approved by the Institutional Review Board of Regierungspräsidium Darmstadt (protocol code V54-19c20/15-FK/1073, date of approval: 28 September 2016).

Data Availability Statement: All primary data were made publicly available via the PeptideAtlas repository with the dataset identifier PASS05856 and the ProteomeXchange Consortium with the dataset identifier PXD048640.

Acknowledgments: We are grateful for the technical assistance of Gabriele Köpf in Frankfurt and of Beata Lukaszewsa-McGreal in Berlin. We thank Hildegard König regarding our biosafety S1/S2 lab and the staff of the animal facility ZFE in Frankfurt/M. We are very grateful to Ilka Wittig and Jana Meisterknecht in the Functional Proteomics team at Goethe University for their excellent mass spectrometry services.

Conflicts of Interest: The authors declare no conflict of interest. The funders had no role in the design of the study; in the collection, analyses, or interpretation of data; in the writing of the manuscript, or in the decision to publish the results.

Abbreviations

2PG	2-phosphoglycerate
5S rRNA	the smallest rRNA within the eukaryotic ribosomal LSU
60S subunit	eukaryotic ribosomal LSU with sedimentation at 60 Svedberg units
AAA+	ATPases associated with various cellular activities
ABAT	4-aminobutyrate aminotransferase
ABC	ammonium bicarbonate
AGAT	= GATM, L-arginine:glycine amidinotransferase
AGC	automatic gain control
AGXT2	alanine-glyoxylate aminotransferase 2
ALA	= deltaALA , delta-amino-levulinic-acid
Ala	alanine
ALAS	delta-amino-levulinic-acid synthase, generic
ALAS1	delta-amino-levulinic-acid synthase 1, non-specific
ALAS2	delta-amino-levulinic-acid synthase 1, erythroid-specific
ALDH18A1	aldehyde dehydrogenase 18 family member A1
Arg	arginine
ASMT	acetylserotonin O-methyltransferase
Asn	asparagine
Asp	aspartate
ATF4	*activating transcription factor 4*
ATP	adenosine trisphosphate
BAG-domain	Bcl-2-associated athanogene-domain
BCAT2	branched chain amino acid transaminase 2
BCL2	BCL2 apoptosis regulator
C1/4/5/6	chain composed of 1/4/5/6 carbons
C57BL/6	inbred substrain 6 generated by C.C. Little, from Abbie Lathrop's mouse 57, with nearly black coat

 doi:10.20944/preprints202401.1423.v1

CI	respiratory chain complex I
CIV	respiratory chain complex IV
Cit	citrulline
CLPA-E	caseinolytic mitochondrial matrix peptidase chaperone subunit A-E
CLPP	caseinolytic mitochondrial matrix peptidase proteolytic subunit
CLPX	caseinolytic mitochondrial matrix peptidase chaperone subunit X
CM liquid medium	complete medium containing glucose monohydrate
Co^{2+}	elemental cobalt as divalent cation
CoA	coenzyme A
COX2	mitochondrially encoded cytochrome C oxidase II
COX7A	cytochrome C oxidase subunit 7A1
COXFA4	= NDUFA4; cytochrome C oxidase subunit FA4
CPOX	coproporphyrinogen oxidase
CPT	carnitine palmitoyltransferase 2
CTP	cytidine trisphosphate
Cys	cysteine
DNA	desoxyribonucleic acid
DnaK	*E. coli* chaperone protein
DTT	dithiothreitol
EARS2	glutamyl-tRNA synthetase 2, mitochondrial
eIF6	eukaryotic translation initiation factor 6
ETNPPL	ethanolamine-phosphate phospho-lyase
ESI	electrospray ionization
ESSS	= NDUFB11, NADH-ubiquinone oxidoreductase subunit B11
FAD	flavin adenine dinucleotide
FC	fold-change
FDR	false discovery rate
Fe^{2+}	ferrous iron = iron(II), elemental iron as divalent cation
FECH	ferrochelatase
FeS clusters	iron-sulfur clusters
G1SA	=GSA, glutamate-1-semialdehyde
G5SA	glutamate-5'-semialdehyde
GABA	gamma-amino-butyric-acid
GAMT	guanidinoacetate N-methyltransferase
GAR1	Gar1 Ribonucleoprotein Homolog
GATC	glutaminyl-tRNA-synthase subunit C, mitochondrial
GATM	glycine amidinotransferase
GDH1	glutamate decarboxylase 1
GFM1/2	translation elongation factor G, mitochondrial, variant 1/2
GH	growth hormone
GLDC	glycine decarboxylase
Gln	glutamine
GltX	glutamate-tRNA ligase
Glu	glutamate
Gly	glycine
GO-term	gene ontology term
GOT1/2	glutamic-oxaloacetic transaminase 1/2
GPT	glutamic-pyruvic transaminase
GSSG	glutathione disulfide
GTP	guanosine triphosphate
H/ACA	sequence motifs H box (consensus ANANNA) and ACA box (ACA)
HARS2	histidine-tRNA ligase, mitochondrial

 doi:10.20944/preprints202401.1423.v1

HemA	glutamyl-tRNA reductase
HemL	**glutamate-1-semialdehyde 2,1-aminomutase**
Hexose-1,6BP	hexose-1,6-bisphosphate
Hexose-6P	hexose-6-phosphate
His	histidine
Hsc70	heat shock cognate 71 kDa protein
Hse	homoserine
HSP70	heat shock protein family A (Hsp70) member 4
i-AAA	mitochondrial intermembrane space AAA+ protease
Ile	isoleucine
kDa	kiloDalton (molecular weight unit)
L7/L12 stalk	stalk structure in the mitoribosomal LSU, composed of proteins 7 / 12
LARS2	leucyl-tRNA synthetase 2, mitochondrial
LC/MS	liquid chromatography / mass spectrometry
Leu	leucine
LMBRD1	lysosomal cobalamin transport escort protein LMBR1
LonP	Lon peptidase 1 homolog, mitochondrial
Lsm7	like-SM domain containing protein 7, cytosolic
LSU	mitoribosomal large subunit
LYRM6	protein 6 with conserved tripeptide (LYR) motif
m3G	2,2,7-trimethyl guanosine
MCX1	yeast CLPX homolog
Met	methionine
Mg^{2+}	elemental magnesium as divalent cation
1-MHis	1-methylhistamine
MRM	multiple reaction mode
MRPP1	= TRMT10C; mitochondrial ribonuclease P protein 1
MRPP3	= PRORP; mitochondrial ribonuclease P protein 3
MS	mass spectrometry
MRPL30	large ribosomal subunit protein uL30m
MRPL33	large ribosomal subunit protein bL33m
MTBE	methyl-tert-butyl ester
mt-CO3	mitochondrially encoded cytochrome C oxidase III
mtDNA	mitochondrial DNA, nucleoid
5,10-MTHF	5,10-methylenetetrahydrofolate
MTHFD2	methylenetetrahydrofolate dehydrogenase (NADP+ dependent) 2, methenyltetrahydrofolate cyclohydrolase.
NADPH	nicotinamide adenine dinucleotide phosphate
NDUFA1	NADH:ubiquinone oxidoreductase subunit A1
NDUFA2	NADH:ubiquinone oxidoreductase subunit A2
NDUFA2	NADH:ubiquinone oxidoreductase subunit A3
NDUFA4	NADH:ubiquinone oxidoreductase subunit A4
NDUFA6	NADH:ubiquinone oxidoreductase subunit A6
NDUFB2	NADH:ubiquinone oxidoreductase subunit B2
NDUFB11	NADH:ubiquinone oxidoreductase subunit B11
NDUFS6	NADH:ubiquinone oxidoreductase subunit S6
NFS1	nitrogen fixing bacteria S-like protein 1, cysteine desulfurase
NOP10	homolog of yeast Nop10p
NTMT1/2	N-terminal Xaa-Pro-Lys N-methyltransferase 1/2
OAT	ornithine aminotransferase
ODC	= ODC1, ornithine decarboxylase 1
ODO1	2-oxoglutarate dehydrogenase complex component E1

 doi:10.20944/preprints202401.1423.v1

ONC201 = dordaviprone: 11-benzyl-7-[(2-methylphenyl)methyl]-2,5,7,11-tetrazatricyclo[7.4.0.02,6]trideca-1(9),5-dien-8-one
Orn ornithine
OTC ornithine transcarbamylase
P5C delta-1-pyrroline-5-carboxylate
P5CDH pyrroline-5-carboxylate dehydrogenase
P5CS pyrroline-5-carboxylate synthetase = ALDH18A1
P5P pyridoxal-5′-phosphate
Pa Podospora anserina fungus
PADI peptidylarginine-deiminases
PAGE polyacrylamide gel electrophoresis
PaIap = B2B020 in UniProt; mitoch. intermembrane space AAA+ protease
PaSnf1 = B2B4C1 in UniProt; sucrose non-fermenting complex, catalytic 1
PEP phosphoenolpyruvate
1,3PG 1,3-bisphospho-glycerate
2PG 2-phosphoglycerate
3PG 3-phosphoglycerate
PHD prolyl-3-hydroxlase domain
Phe phenylalanine
PHYKPL 5-phosphohydroxy-L-lysine phospho-lyase
PLP pyridoxal-5′-phosphate
PodAns Podospora anserina fungus
PP/PE polypropylene/polyehtylene
PPIX protoporphyrinogen IX
PRLTS3 Perrault syndrome type 3
Pro proline
PRORP protein only RNase P catalytic subunit
RMND1 required for meiotic nuclear division 1 homolog
RNA ribonucleic acid
rRNA ribosomal RNA
SAM S-adenosyl-methionine
SAM-MTases S-adenosyl-methionine-dependent methyltransferases
SAP domain DNA-binding 35-residue motif, named after SAF-A/B, Acinus and PIAS, three proteins known to contain it
SDS sodium dodecyl sulfate
Ser serine
SHMT2 serine hydroxymethyltransferase 2, mitochondrial
Sm domain occur in Sm proteins, named in honor of patient Stephanie Smith
SmG-like domain spliceosomal core protein SmG, binding to AU-dinucleotide
snoRNA small nucleolar *RNA*
snRNA small nuclear RNA
snRNP small nuclear ribonucleoprotein
SSU ribosomal small subunit
STRING search tool for the retrieval of interacting genes/proteins
Tae1 alpha N-terminal protein methyltransferase 1
TCA cycle tricarboxylic acid cycle
Thr threonine
TRMT10C tRNA methyltransferase 10C, mitochondrial RNase P mubunit
tRNA transfer RNA
$tRNA^{Val/Phe}$ transfer RNA for valine or phenylalanine
Trp tryptophan
TWNK twinkle

Tyr	tyrosine
UniProt	public database about proteins, unifying nomenclature
UniProt-ID	UniProt protein identifier number
UPR^{mt}	mitochondrial unfolded protein response
UTP	uridine triphosphate
v/v	volume per volume
WT	wildtype
ZFE	Zentrale Forschungs-Einrichtung

References

1. Olivares, A.O., T.A. Baker, and R.T. Sauer, *Mechanistic insights into bacterial AAA+ proteases and protein-remodelling machines.* Nat Rev Microbiol, 2016. **14**(1): p. 33-44.
2. Huang, S., J. Petereit, and A.H. Millar, Loss of conserved mitochondrial CLPP and its functions lead to different phenotypes in plants and other organisms. Plant Signal Behav, 2020. **15**(12): p. 1831789.
3. Auburger, G., J. Key, and S. Gispert, The Bacterial ClpXP-ClpB Family Is Enriched with RNA-Binding Protein Complexes. Cells, 2022. **11**(15).
4. Mabanglo, M.F., V. Bhandari, and W.A. Houry, *Substrates and interactors of the ClpP protease in the mitochondria.* Curr Opin Chem Biol, 2022. **66**: p. 102078.
5. Key, J., et al., Global Proteome of LonP1(+/-) Mouse Embryonal Fibroblasts Reveals Impact on Respiratory Chain, but No Interdependence between Eral1 and Mitoribosomes. Int J Mol Sci, 2019. **20**(18).
6. Chandu, D. and D. Nandi, Comparative genomics and functional roles of the ATP-dependent proteases Lon and Clp during cytosolic protein degradation. Res Microbiol, 2004. **155**(9): p. 710-9.
7. Maurizi, M.R., et al., Sequence and structure of Clp P, the proteolytic component of the ATP-dependent Clp protease of Escherichia coli. J Biol Chem, 1990. **265**(21): p. 12536-45.
8. Gispert, S., et al., Loss of mitochondrial peptidase Clpp leads to infertility, hearing loss plus growth retardation via accumulation of CLPX, mtDNA and inflammatory factors. Hum Mol Genet, 2013. **22**(24): p. 4871-87.
9. Froese, D.S., B. Fowler, and M.R. Baumgartner, Vitamin B(12) , folate, and the methionine remethylation cycle-biochemistry, pathways, and regulation. J Inherit Metab Dis, 2019. **42**(4): p. 673-685.
10. Kardon, J.R., et al., Mitochondrial ClpX Activates a Key Enzyme for Heme Biosynthesis and Erythropoiesis. Cell, 2015. **161**(4): p. 858-67.
11. van der Vorm, L.N. and B.H. Paw, *Studying disorders of vertebrate iron and heme metabolism using zebrafish.* Methods Cell Biol, 2017. **138**: p. 193-220.
12. Yien, Y.Y., et al., Mutation in human CLPX elevates levels of delta-aminolevulinate synthase and protoporphyrin IX to promote erythropoietic protoporphyria. Proc Natl Acad Sci U S A, 2017. **114**(38): p. E8045-E8052.
13. Ducamp, S., et al., A mutation in the iron-responsive element of ALAS2 is a modifier of disease severity in a patient suffering from CLPX associated erythropoietic protoporphyria. Haematologica, 2021. **106**(7): p. 2030-2033.
14. Shemin, D., An illustration of the use of isotopes: the biosynthesis of porphyrins. Bioessays, 1989. **10**(1): p. 30-5.
15. Beale, S.I. and P.A. Castelfranco, The Biosynthesis of delta-Aminolevulinic Acid in Higher Plants: II. Formation of C-delta-Aminolevulinic Acid from Labeled Precursors in Greening Plant Tissues. Plant Physiol, 1974. **53**(2): p. 297-303.
16. Iida, K., I. Mimura, and M. Kajiwara, Evaluation of two biosynthetic pathways to delta-aminolevulinic acid in Euglena gracilis. Eur J Biochem, 2002. **269**(1): p. 291-7.
17. Petricek, M., et al., Occurrence of two 5-aminolevulinate biosynthetic pathways in Streptomyces nodosus subsp. asukaensis is linked with the production of asukamycin. J Bacteriol, 2006. **188**(14): p. 5113-23.
18. Key, J., et al., Translation fidelity and respiration deficits in CLPP-deficient tissues: Mechanistic insights from mitochondrial complexome. Int J Mol Sci, 2023. **24**(24): p. 17503.
19. Koper, K., et al., Evolutionary origin and functional diversification of aminotransferases. J Biol Chem, 2022. **298**(8): p. 102122.
20. Cellini, B., et al., The chaperone role of the pyridoxal 5'-phosphate and its implications for rare diseases involving B6-dependent enzymes. Clin Biochem, 2014. **47**(3): p. 158-65.
21. Liang, J., et al., Current Advances on Structure-Function Relationships of Pyridoxal 5'-Phosphate-Dependent Enzymes. Front Mol Biosci, 2019. **6**: p. 4.
22. Shin, B.S., et al., Amino acid substrates impose polyamine, eIF5A, or hypusine requirement for peptide synthesis. Nucleic Acids Res, 2017. **45**(14): p. 8392-8402.
23. Pegg, A.E., *Toxicity of polyamines and their metabolic products.* Chem Res Toxicol, 2013. **26**(12): p. 1782-800.

24. di Salvo, M.L., N. Budisa, and R. Contestabile, *PLP-dependent Enzymes: a Powerful Tool for Metabolic Synthesis of Non-canonical Amino Acids.* https://www.beilstein-institut.de/download/65/plp-dependent_enzymes_a_powerful_tool_for_metabolic_synthesis_of_non-canonical_amino_acids_.pdf, 2012.
25. Obermaier, S. and M. Muller, Ibotenic Acid Biosynthesis in the Fly Agaric Is Initiated by Glutamate Hydroxylation. Angew Chem Int Ed Engl, 2020. **59**(30): p. 12432-12435.
26. Chen, M., C.T. Liu, and Y. Tang, Discovery and Biocatalytic Application of a PLP-Dependent Amino Acid gamma-Substitution Enzyme That Catalyzes C-C Bond Formation. J Am Chem Soc, 2020. **142**(23): p. 10506-10515.
27. Haynes, C.M., et al., ClpP mediates activation of a mitochondrial unfolded protein response in C. elegans. Dev Cell, 2007. **13**(4): p. 467-80.
28. Zhou, Z., et al., The mitochondrial unfolded protein response: A multitasking giant in the fight against human diseases. Ageing Res Rev, 2022. **81**: p. 101702.
29. Al-Furoukh, N., et al., ClpX stimulates the mitochondrial unfolded protein response (UPRmt) in mammalian cells. Biochim Biophys Acta, 2015. **1853**(10 Pt A): p. 2580-91.
30. Levchenko, I., et al., A specificity-enhancing factor for the ClpXP degradation machine. Science, 2000. **289**(5488): p. 2354-6.
31. Lytvynenko, I., et al., Alanine Tails Signal Proteolysis in Bacterial Ribosome-Associated Quality Control. Cell, 2019. **178**(1): p. 76-90 e22.
32. Wu, Z., et al., MISTERMINATE Mechanistically Links Mitochondrial Dysfunction with Proteostasis Failure. Mol Cell, 2019. **75**(4): p. 835-848 e8.
33. Huter, P., et al., Structural Basis for Polyproline-Mediated Ribosome Stalling and Rescue by the Translation Elongation Factor EF-P. Mol Cell, 2017. **68**(3): p. 515-527 e6.
34. Konovalova, S., et al., Exposure to arginine analog canavanine induces aberrant mitochondrial translation products, mitoribosome stalling, and instability of the mitochondrial proteome. Int J Biochem Cell Biol, 2015. **65**: p. 268-74.
35. Ou, X., et al., Errors in translational decoding: tRNA wobbling or misincorporation? PLoS Genet, 2019. **15**(3): p. e1008017.
36. Jenkinson, E.M., et al., Perrault syndrome is caused by recessive mutations in CLPP, encoding a mitochondrial ATP-dependent chambered protease. Am J Hum Genet, 2013. **92**(4): p. 605-13.
37. Newman, W.G., et al., *Perrault Syndrome*, in *GeneReviews((R))*, M.P. Adam, et al., Editors. 1993: Seattle (WA).
38. Theunissen, T.E., et al., Specific MRI Abnormalities Reveal Severe Perrault Syndrome due to CLPP Defects. Front Neurol, 2016. **7**: p. 203.
39. Key, J., et al., Inactivity of Peptidase ClpP Causes Primary Accumulation of Mitochondrial Disaggregase ClpX with Its Interacting Nucleoid Proteins, and of mtDNA. Cells, 2021. **10**(12).
40. Faridi, R., et al., New insights into Perrault syndrome, a clinically and genetically heterogeneous disorder. Hum Genet, 2022. **141**(3-4): p. 805-819.
41. Hochberg, I., et al., Bi-allelic variants in the mitochondrial RNase P subunit PRORP cause mitochondrial tRNA processing defects and pleiotropic multisystem presentations. Am J Hum Genet, 2021. **108**(11): p. 2195-2204.
42. Bhandari, V., et al., The Role of ClpP Protease in Bacterial Pathogenesis and Human Diseases. ACS Chem Biol, 2018. **13**(6): p. 1413-1425.
43. Prabhu, V.V., et al., ONC201 and imipridones: Anti-cancer compounds with clinical efficacy. Neoplasia, 2020. **22**(12): p. 725-744.
44. Zhang, R., et al., Assessment of the structure-activity relationship and antileukemic activity of diacylpyramide compounds as human ClpP agonists. Eur J Med Chem, 2023. **258**: p. 115577.
45. Key, J., et al., CLPP Depletion Causes Diplotene Arrest; Underlying Testis Mitochondrial Dysfunction Occurs with Accumulation of Perrault Proteins ERAL1, PEO1, and HARS2. Cells, 2022. **12**(1).
46. Bhaskaran, S., et al., Loss of mitochondrial protease ClpP protects mice from diet-induced obesity and insulin resistance. EMBO Rep, 2018. **19**(3).
47. Becker, C., et al., CLPP deficiency protects against metabolic syndrome but hinders adaptive thermogenesis. EMBO Rep, 2018. **19**(5).
48. Szczepanowska, K., et al., CLPP coordinates mitoribosomal assembly through the regulation of ERAL1 levels. EMBO J, 2016. **35**(23): p. 2566-2583.
49. Key, J., et al., Loss of mitochondrial ClpP, Lonp1, and Tfam triggers transcriptional induction of Rnf213, a susceptibility factor for moyamoya disease. Neurogenetics, 2020. **21**(3): p. 187-203.
50. Torres-Odio, S., et al., Loss of Mitochondrial Protease CLPP Activates Type I IFN Responses through the Mitochondrial DNA-cGAS-STING Signaling Axis. J Immunol, 2021. **206**(8): p. 1890-1900.
51. Maletzko, A., et al., Increased presence of nuclear DNAJA3 and upregulation of cytosolic STAT1 and of nucleic acid sensors trigger innate immunity in the ClpP-null mouse. Neurogenetics, 2021. **22**(4): p. 297-312.

52. Osiewacz, H.D., Mitochondrial quality control in aging and lifespan control of the fungal aging model Podospora anserina. Biochem Soc Trans, 2011. **39**(5): p. 1488-92.
53. Osiewacz, H.D., A. Hamann, and S. Zintel, Assessing Organismal Aging in the Filamentous Fungus Podospora anserina, in Cell Senescence: Methods and Protocols, Methods in Molecular Biology, L. Galluzzi, et al., Editors. 2013, Humana: Totowa, NJ.
54. Fischer, F., et al., Human CLPP reverts the longevity phenotype of a fungal ClpP deletion strain. Nat Commun, 2013. **4**: p. 1397.
55. Heinz, D., et al., Simultaneous Ablation of the Catalytic AMPK alpha-Subunit SNF1 and Mitochondrial Matrix Protease CLPP Results in Pronounced Lifespan Extension. Front Cell Dev Biol, 2021. **9**: p. 616520.
56. Fischer, F., J.D. Langer, and H.D. Osiewacz, Identification of potential mitochondrial CLPXP protease interactors and substrates suggests its central role in energy metabolism. Sci Rep, 2015. **5**: p. 18375.
57. Szczepanowska, K., et al., A salvage pathway maintains highly functional respiratory complex I. Nat Commun, 2020. **11**(1): p. 1643.
58. Petereit, J., et al., Mitochondrial CLPP2 Assists Coordination and Homeostasis of Respiratory Complexes. Plant Physiol, 2020. **184**(1): p. 148-164.
59. Meierhofer, D., et al., Ataxin-2 (Atxn2)-Knock-Out Mice Show Branched Chain Amino Acids and Fatty Acids Pathway Alterations. Mol Cell Proteomics, 2016. **15**(5): p. 1728-39.
60. Gielisch, I. and D. Meierhofer, Metabolome and proteome profiling of complex I deficiency induced by rotenone. J Proteome Res, 2015. **14**(1): p. 224-35.
61. Funck, D., B. Stadelhofer, and W. Koch, Ornithine-delta-aminotransferase is essential for arginine catabolism but not for proline biosynthesis. BMC Plant Biol, 2008. **8**: p. 40.
62. Du, J., et al., Proline metabolism and transport in retinal health and disease. Amino Acids, 2021. **53**(12): p. 1789-1806.
63. Monne, M., et al., Mitochondrial transport and metabolism of the major methyl donor and versatile cofactor S-adenosylmethionine, and related diseases: A review(dagger). IUBMB Life, 2022. **74**(7): p. 573-591.
64. Rebelo-Guiomar, P., et al., A late-stage assembly checkpoint of the human mitochondrial ribosome large subunit. Nat Commun, 2022. **13**(1): p. 929.
65. Koditz, J., et al., Oxygen-dependent ATF-4 stability is mediated by the PHD3 oxygen sensor. Blood, 2007. **110**(10): p. 3610-7.
66. Stranska, J., et al., Ornithine delta-aminotransferase: An enzyme implicated in salt tolerance in higher plants. Plant Signal Behav, 2008. **3**(11): p. 929-35.
67. Llacer, J.L., I. Fita, and V. Rubio, *Arginine and nitrogen storage.* Curr Opin Struct Biol, 2008. **18**(6): p. 673-81.
68. Pencharz, P.B., *Assessment of protein nutritional status in children.* Pediatr Blood Cancer, 2008. **50**(2 Suppl): p. 445-6; discussion 451.
69. Sodero, G., et al., Growth hormone responses during arginine and clonidine stimulation test: Correlations with patients' auxological and metabolic parameters in a single centre study. Growth Horm IGF Res, 2023. **68**: p. 101522.
70. Stefani, G.P., et al., Resistance training and L-arginine supplementation are determinant in genomic stability, cardiac contractility and muscle mass development in rats. PLoS One, 2018. **13**(9): p. e0204858.
71. Vanderniet, J.A., et al., Barth syndrome with severe dilated cardiomyopathy and growth hormone resistance: a case report. J Pediatr Endocrinol Metab, 2021. **34**(7): p. 951-955.
72. Brown, A., et al., Structure of the large ribosomal subunit from human mitochondria. Science, 2014. **346**(6210): p. 718-722.
73. Miluzio, A., et al., Eukaryotic initiation factor 6 mediates a continuum between 60S ribosome biogenesis and translation. EMBO Rep, 2009. **10**(5): p. 459-65.
74. Gartmann, M., et al., Mechanism of eIF6-mediated inhibition of ribosomal subunit joining. J Biol Chem, 2010. **285**(20): p. 14848-14851.
75. Weis, F., et al., Mechanism of eIF6 release from the nascent 60S ribosomal subunit. Nat Struct Mol Biol, 2015. **22**(11): p. 914-9.
76. Jaako, P., et al., eIF6 rebinding dynamically couples ribosome maturation and translation. Nat Commun, 2022. **13**(1): p. 1562.
77. Pesce, E., et al., Discovery and Preliminary Characterization of Translational Modulators that Impair the Binding of eIF6 to 60S Ribosomal Subunits. Cells, 2020. **9**(1).
78. Balogh, E., et al., Pseudouridylation defect due to DKC1 and NOP10 mutations causes nephrotic syndrome with cataracts, hearing impairment, and enterocolitis. Proc Natl Acad Sci U S A, 2020. **117**(26): p. 15137-15147.
79. De Zoysa, M.D. and Y.T. Yu, *Posttranscriptional RNA Pseudouridylation.* Enzymes, 2017. **41**: p. 151-167.
80. Jakubowski, H., Misacylation of tRNALys with noncognate amino acids by lysyl-tRNA synthetase. Biochemistry, 1999. **38**(25): p. 8088-93.
81. Bauerle, M.R., E.L. Schwalm, and S.J. Booker, *Mechanistic diversity of radical S-adenosylmethionine (SAM)-dependent methylation.* J Biol Chem, 2015. **290**(7): p. 3995-4002.

82. Webb, K.J., et al., Identification of protein N-terminal methyltransferases in yeast and humans. Biochemistry, 2010. **49**(25): p. 5225-35.
83. Bhatta, A., et al., *Structural basis of RNA processing by human mitochondrial RNase P.* Nat Struct Mol Biol, 2021. **28**(9): p. 713-723.
84. Metodiev, M.D., et al., Recessive Mutations in TRMT10C Cause Defects in Mitochondrial RNA Processing and Multiple Respiratory Chain Deficiencies. Am J Hum Genet, 2016. **98**(5): p. 993-1000.
85. Averbeck, N.B., et al., Identification and characterization of PaMTH1, a putative O-methyltransferase accumulating during senescence of Podospora anserina cultures. Curr Genet, 2000. **37**(3): p. 200-8.
86. Kunstmann, B. and H.D. Osiewacz, Over-expression of an S-adenosylmethionine-dependent methyltransferase leads to an extended lifespan of Podospora anserina without impairments in vital functions. Aging Cell, 2008. **7**(5): p. 651-62.
87. Kunstmann, B. and H.D. Osiewacz, The S-adenosylmethionine dependent O-methyltransferase PaMTH1: a longevity assurance factor protecting Podospora anserina against oxidative stress. Aging (Albany NY), 2009. **1**(3): p. 328-34.
88. Knab, B. and H.D. Osiewacz, Methylation of polyphenols with vicinal hydroxyl groups: A protection pathway increasing organismal lifespan. Cell Cycle, 2010. **9**(17): p. 3387-8.
89. Chatterjee, D., et al., Structure and Biophysical Characterization of the S-Adenosylmethionine-dependent O-Methyltransferase PaMTH1, a Putative Enzyme Accumulating during Senescence of Podospora anserina. J Biol Chem, 2015. **290**(26): p. 16415-30.
90. Madeo, F., et al., *Spermidine in health and disease.* Science, 2018. **359**(6374).
91. Gailus, S., et al., Insights into lysosomal cobalamin trafficking: lessons learned from cblF disease. J Mol Med (Berl), 2010. **88**(5): p. 459-66.
92. Balsa, E., et al., NDUFA4 is a subunit of complex IV of the mammalian electron transport chain. Cell Metab, 2012. **16**(3): p. 378-86.
93. Kadenbach, B., Regulation of Mammalian 13-Subunit Cytochrome c Oxidase and Binding of other Proteins: Role of NDUFA4. Trends Endocrinol Metab, 2017. **28**(11): p. 761-770.
94. Yagil, C., R. Varadi-Levi, and Y. Yagil, A novel mutation in the NADH dehydrogenase (ubiquinone) 1 alpha subcomplex 4 (Ndufa4) gene links mitochondrial dysfunction to the development of diabetes in a rodent model. Dis Model Mech, 2018. **11**(11).
95. Kadenbach, B., Complex IV - The regulatory center of mitochondrial oxidative phosphorylation. Mitochondrion, 2021. **58**: p. 296-302.
96. Sorouri, M., et al., Signatures of host-pathogen evolutionary conflict reveal MISTR-A conserved MItochondrial STress Response network. PLoS Biol, 2020. **18**(12): p. e3001045.
97. Hock, D.H., D.R.L. Robinson, and D.A. Stroud, Blackout in the powerhouse: clinical phenotypes associated with defects in the assembly of OXPHOS complexes and the mitoribosome. Biochem J, 2020. **477**(21): p. 4085-4132.
98. Letts, J.A., K. Fiedorczuk, and L.A. Sazanov, *The architecture of respiratory supercomplexes.* Nature, 2016. **537**(7622): p. 644-648.
99. Guerrero-Castillo, S., et al., *The Assembly Pathway of Mitochondrial Respiratory Chain Complex I.* Cell Metab, 2017. **25**(1): p. 128-139.
100. Signes, A. and E. Fernandez-Vizarra, Assembly of mammalian oxidative phosphorylation complexes I-V and supercomplexes. Essays Biochem, 2018. **62**(3): p. 255-270.
101. Formosa, L.E., et al., Building a complex complex: Assembly of mitochondrial respiratory chain complex I. Semin Cell Dev Biol, 2018. **76**: p. 154-162.
102. Giachin, G., et al., Dynamics of Human Mitochondrial Complex I Assembly: Implications for Neurodegenerative Diseases. Front Mol Biosci, 2016. **3**: p. 43.